Characteristics of ozone and particles in the near-surface atmosphere in urban area of the Yangtze River Delta, China

Huimin Chen[1], Bingliang Zhuang[1,*], Jane Liu[1,2], TijianWang[1,**], Shu Li[1], Min Xie[1], Mengmeng Li[1], Pulong Chen[1], Ming Zhao[1]

[1]School of Atmospheric Sciences, CMA-NJU Joint Laboratory for Climate Prediction Studies, Jiangsu Collaborative Innovation Center for Climate Change, Nanjing University, Nanjing 210023, China

[2]Department of Geography and Planning, University of Toronto, Toronto, M5S 3G3, Canada

Correspondence: Bingliang Zhuang (blzhuang@nju.edu.cn) and Tijian Wang (tjwang@nju.edu.cn)

Abstract

Aerosols and ozone have significant influences on air qualities, human health and climate changes. To further understand the characteristics and interactions among different urban air pollutants in the west Yangtze River Delta (YRD) region, continuous measurements of low layer atmospheric particles and trace gases have been performed at an urban site in Nanjing from September 2016 to February 2017 in this study. In urban area of west YRD, the mean PM_{10} and O_3 concentrations are 86.3 μg/m^3 and 37.7 ppb, respectively, with significant seasonal and diurnal variations. Particles, which are dominated by fine aerosols, are relatively scattering. And most of their optical properties have the similar variations to the aerosol concentrations. Results also show that west YRD could still suffer severe air pollutions, although the seasonal mean aerosol concentrations have been decreased in recent years. Even in cold seasons, O_3 could have about 40 days excess against to the National Ambient Air Quality Standards during the sampling period. Most of polluted episodes are

caused by local and sub-regional emissions. A case study for a typical O_3 and $PM_{2.5}$ episode in December 2016 demonstrates that the episode was generally associated with regional transport and stable weather system. Air pollutants were mostly transported from the western areas with high emissions, as well as with an anticyclone and high-pressure system in this region. Correlation analysis revels that the interaction between O_3 and PMs are complex with a combination of inhibition and promotion under different conditions. The inhibition effect might result from the reduction of photolysis frequency near surface due to aerosols besides their positive correlations with precursors, while the promotion effect is from the formation of secondary aerosols under high concentrations of oxidants and solar radiation. However, the interaction between O_3 and BC shows an inhibit effect due to its chemical stability. It is also indicated a VOC-sensitive regime for photochemical production of O_3 in this region. This study further improves the insight in the characteristics and interactions of main pollutants, and might have a certain contribution to improve the simulation and prediction of aerosols and gases in urban area of YRD.

~~To improve the understanding of the interactions between particles and trace gases in a typical city of the YRD region, continuous measurements of particles and trace gases were made at an urban site in Nanjing during cold seasons in 2016 in this study. The average of particles, including black carbon (BC), $PM_{2.5}$, and PM_{10} are 2.602±1.720 μg/m^3, 58.2±36.8 μg/m^3, and 86.3±50.8 μg/m^3, respectively, while the average of trace gases, which contain CO, O_3, NO_x, and NO_y, are 850.9±384.1, 37.7±33.5, 23.5±14.7, and 32.8±22.3 ppb, respectively. Compared to National Ambient Air Quality Standards in China (NAAQS-CN), we found 48 days excess of $PM_{2.5}$, 14 days excess of PM_{10}, and 40 days excess of O_3. The particles, CO, and nitrogen oxide concentrations shared a similar pattern of seasonality and diurnal cycles, which are different from O_3. The former ones are~~

~~all high in DJF and at rush hours, while the latter one had high loadings in the daytime, especially when the ultra violet (UV) was high. Correlation analysis reveals the formation of secondary aerosols, especially $PM_{2.5}$, under high O_3 and temperature conditions, and suggests a VOC-sensitive regime for photochemical production of O_3 in urban Nanjing in cold seasons. Backward trajectory analysis suggests the prevailing winds in Nanjing were northerly and easterly during cold seasons in 2016. Air masses from eastern without passing through the urban agglomeration and those from northern without crossing BTH regions were cleaner, but air masses from local regions were more polluted in winter. A case study for a typical O_3 and $PM_{2.5}$ episode in December 2016 demonstrated that the episode was generally associated with regional transport and stable weather system. Air pollutants were mostly transported from the western areas with high emissions and weather conditions are controlled by anticyclone and high-pressure system in this region. This study further reveals the important effects of weather system and human activities on the environment in the YRD region, especially in the urban areas, and it's an urgent need for improving air quality in these areas.~~

1. Introduction

Particles, including black carbon (BC), $PM_{2.5}$, and PM_{10}, and trace gases, such as carbon monoxide (CO), ozone (O_3), nitric oxide and nitrogen dioxide (NO_x), and total reactive nitrogen (NO_y, which includes NO_x, aerosol nitrates (NO_3^-), nitric acid (HNO_3), N_2O_5, peroxyacetyl nitrate (PAN), and various nitrogen-containing organic compounds.), are important components in the troposphere because of their impacts on human health, biosphere and climate changes (e.g., Chameides et al., 1999a, b; Jerrett et al., 2009; Allen et al., 2012). Through long-range particle cycles, particles could

interact with atmospheric trace gases from complex sources, especially ozone and its precursors, disturbing the earth's radiation budget (Sassen, 2002), or providing reactive surfaces for heterogeneous reactions (Kumar et al., 2014), which leads to a great but hard problem for regional air quality (Zhang et al., 2008; van Donkelaar et al., 2010). ~~BC is mostly from incomplete combustion of coal, diesel fuels, biofuels, and outdoor biomass burning (Bond et al., 2004). Although BC accounts for a relatively small portion of the total mass concentrations of aerosol particles in atmosphere, it plays a significant role in global radiation balance, both directly and indirectly. Thus, BC could influence the global and region climate changes and atmospheric environment substantially (Jacobson et al., 2002; Bond et al., 2013; Deng et al., 2010). Particulate matters (PMs) originate from both natural and anthropogenic emission sources (Kaufman et al., 2002). Due to prosperous economic development, rapid industrialization and urbanization in recent decades, haze events have frequently occurred in the Beijing-Tianjin-Hebei (BTH) area, Yangtze River Delta (YRD) and Pearl River Delta (PRD) regions, all of which were mainly caused by high concentrations of particulate matter. Tropospheric ozone is a typical secondary air pollutant that is related to its precursors NOx and VOCs (Crutzen, 1973) through several complicated reactions. O_3 could impact tropospheric environment (Monks et al., 2015), and make significant contributions to radiative forcing of climate (Intergovernmental Panel on Climate Change (IPCC), 2007). Tropospheric O_3 precursors and the interactions between O_3 and its precursors in different geographical locations are usually different, and thereby the characterizations of O_3 at different sites can vary greatly (Xie et al., 2016). The impact of PMs and BC on surface ozone is a topic that has attracted much attention. Jacobson (1998) reported that aerosols containing BC cores reduced photolysis rates and resulted in a decrease in ozone concentrations by 5%–8% at ground level in~~

~~Los Angeles. It is also found that a strong reduction in photolysis rate (10%–30%) due to BC-containing aerosols (Castro et al., 2001) led to a decrease in surface ozone in Mexico City. Similar results have been found in other studies simulating the effects of BC on surface ozone in China (Li et al., 2011).~~

–Over the decades, China is always one of the major source regions of particles, with BC and dust emission accounting for up to 25% of the global anthropogenic sources (Streets et al., 2001; Tegen and Schepanski, 2009). Relatively high levels of particle concentrations are mainly distributed in Beijin-Tianjin-Hebei area (BTH), Yangtze River Delta (YRD), and Pearl River Delta (PRD) regions (e.g., Zhang et al., 2008, 2012; Zhang et al., 2015), along with the rapid economic development. These regions consistently have the highest emissions of anthropogenic precursors (e.g., Wang et al., 2015; Wang et al., 2009b; Ding et al., 2013b; Zheng et al., 2010), which have led to severe region-wide air pollution. Earlier studies on particles mostly focused on concentrations estimation, the chemical characteristics, potential sources, as well as climate effects based on numerical simulations (e.g., Wu et al., 2012; Song et al., 2014; Xiao et al., 2012; Yu et al., 2015; Kristjánsson, 2002; Liao and Seinfeld, 2005; Zhuang et al., 2010, 2013, 2013b, 2018). However, a better understanding of spatial and temporal variations of particles can contribute to the adoption of effective measures to reduce air pollution, and real-time monitoring data is essential to better obtain the detailed variations (seasonal, monthly, and diurnal) on the city scale. In China, the research based on PMs observations, especially in the polluted regions above, have gradually expanded since 2012 due to the establishment of China's $PM_{2.5}$ air quality standards and gradual developments of nationwide PMs observation. The research is mainly related to the temporal and spatial distribution characteristics (e.g., Wang et al., 2015; Chen et al., 2016; Wu et al., 2012), and the effects of meteorological variables on aerosols (e.g., Zhang et al., 2015; Yan et al., 2016; Huang et al., 2015). In addition, many observations of BC have been made in the recent years, most of which concentrated on the analysis of the concentration level and the temporal and spatial variations (e.g., Verma et al., 2010; Wang et al., 2011b; Zhang et al., 2012). Some also revealed the correlations of carbonaceous aerosols (Pan et al., 2011; Zhuang et al., 2014b). Besides particles, because of the lack

of nationwide O_3 monitoring data in earlier years, O_3 and its precursors (NO_x, NO_y, CO and VOCs etc.) pollution situations can only be discerned from limited campaign-type measurements in certain developed regions, for instance, Beijing in BTH area (Shao et al., 2006; Lin et al.,2008; Meng et al., 2009), Guangzhou in PRD region (Zhang et al., 1998; Wang et al., 2003) and Lin'an in YRD region (Luo et al., 2000; Cheung and Wang 2001; Wang et al. 2001a, 2002, 2004; Guo et al. 2004b). Since 2005, the number of photochemical studies through observation data has increased in the PRD region in the south (Xue et al., 2014a), the BTH area in the north (Han, 2011), and the YRD region in the east (Shi et al., 2015). However, large gaps and uncertainties remain in the knowledge of characteristics of regional particles and O_3 pollution and its mitigation strategies due to the complexity of main sources, interaction between different aerosols, and changing meteorology filed.

~~Most of earlier studies on particles were focused on concentrations estimation, the chemical characteristics, potential sources, as well as climate effects of particulate matters based on numerical simulations (Wu et al., 2012; Song et al., 2014; Xiao et al., 2012; Yu et al., 2015; Kristjánsson, 2002; Liao and Seinfeld, 2005; Zhuang et al., 2010; 2013), while observation-based studies of particles were relatively limited. In addition, although a good understanding of the characteristics of O_3 have been gained in the BTH area and the PRD region (Wang et al., 2009; Zheng et al., 2010; Lin et al., 2008) due to a relatively long history of research limited in the megacities, in the YRD region, there were only very limited studies of O_3 made in urban areas in some YRD cities (Tu et al., 2007; Ding et al., 2013; Xie et al., 2016), most of which were based on studies of O_3 measurement beginning in the 1990s at Lin'an site, a rural region in the southeast YRD (Luo et al., 2000). And most of studies in YRD on particles, or particulate matter, were done in the eastern YRD, close to Shanghai, and mainly covered short periods of time. In the YRD region, the prevailing winds are from between the northeast and southeast. Therefore, western YRD region is under a downwind condition. As only few measurement studies have been conducted for western YRD (Tu et al., 2007), large~~

~~knowledge gaps still exist in our understanding of the characteristics and main sources of O_3 and particles (Ding et al., 2013) in the region, let alone their interactions.~~

~~China is always one of the major source regions of particles. Over recent decades, along with the rapid economic development and the growing demand of energy consumption, many areas in China are suffering from the elevated O_3 pollution. In the BTH area, the YRD region, and the PRD region, all of which are the economically vibrant and densely populated, high levels of ozone precursor emissions and O_3 pollution have become one of the major environment problems affecting the public (Chan and Yao, 2008; Zhang et al., 2009; Ma et al., 2012; Xie et al., 2016). Because of complex sources and chemical reactions, and relatively long atmospheric lifetimes of the pollutants in the atmosphere that favors regional and long-range transport, all the pollutants are of great concern for regional air quality but are very difficult to control (Cooper et al., 2005; Zhang et al., 2008).~~ The YRD is located in the eastern part of the Yangtze River Plain, adjacent to the most polluted North China Plain, including large cities of Shanghai, southern Jiangsu and northern Zhejiang. Taking up only 2 percent of the land area in China, this region produces over 20 percent of China's Gross Domestic Product (GDP). Nanjing, as the capital of Jiangsu Province, lies in the middle of YRD. It covers an area over 6000 km^2, with more than 7.3 million residents (http://www.njtj.gov.cn/). Being the second largest commercial center after Shanghai in YRD, even the East China, Nanjing is highly urbanized and industrialized, especially the urban area. In addition, the complex monsoon and synoptic weather may play an important role in air pollution transport and formation in Nanjing. Therefore, the urban atmosphere in Nanjing is also heavily polluted by local emissions and long-distance transport of pollutants, which affects regional climate and air quality (Huang et al., 2013;

Yi et al., 2015). ~~Both particles and O_3 concentrations are found to be high in Nanjing, which affects regional climate and air quality (Zhang et al., 2009; Yi et al., 2015). Therefore~~Thus, the issue of air pollution in Nanjing deserves attentions. Previous studies using observation data in Nanjing often concentrated on characteristics of one of the particles (Deng et al., 2011; Shen et al., 2014; Zhuang et al., 2014b) or ozone and its precursors (Tu et al., 2007; Wang et al., 2008; An et al., 2015), describing the temporal and spatial distributions, and the influence of meteorological effects, but lay less emphasis on the inter-species correlations and the combined effects of pollutants during severe pollution episodes. Ding et al. (2013b) described the characteristics of O_3 and $PM_{2.5}$ with near-surface observation data in rural Nanjing, but the detailed characteristics in urban Nanjing is not clear enough so far.

To fill the knowledge gap, continuous online measurements of particles, trace gases, and other relevant parameters were carried out at Gulou site in urban Nanjing about 80m above the ground, an integrated measurement platform for the study of atmospheric environment and climate change. In this study, 6-month measurement of particles, trace gases, and other related variables at this site during September 2016~ February 2017 when air pollution occurred frequently is analyzed. Our work gives a synthetic analysis about their characteristics. The emphasis of our objective is to improve the insight in the characteristics, interactions of main pollutants, and the influence of integrated meteorology variables based on the observation data at an urban site above ground, and further investigate the possible underlying reasons and mechanisms. Firstly, an in-depth discussion on particles variations is performed, not limited to the concentrations but taking optical properties into consideration as well, to quantify the polluted level in detail. Secondly, a detailed description of O_3 variations can also be found in our study, including the analysis of the main precursors as trace gases (NO_x, NO_y and CO), to have a general and quantitative insight in O_3 pollution situations. Both of the pollutants are analyzed considering the effects of meteorology variables including but not limited to precipitation and temperature. Thirdly, analysis of inter-species correlations gives a

relatively thorough overview of the interactions among various species, and deduction of the underlying chemical mechanisms based on the results of our study and previous studies is also presented in our study. Moreover, backward trajectories analysis is conducted for improving the knowledge of regional/sub-regional transport process in urban Nanjing. Finally, a case study for high particles and O_3 episode is implementing to emphasize the integrated influence of meteorological field on regional air pollution.

In the following, we describe the methodology in Section 2, which includes the measurement site and instruments. Results and discussions are presented in Section 3, consisting of overall temporal variation, correlation analysis, backward trajectory analysis, and case studies. A summary is given in Section 4.

~~In this study, continuous observations of particles, trace gases and certain aerosol optical properties at an urban station in Nanjing (a typical developing city in YRD) have been made in order to characterize the air pollution in the city. In the following, we describe the methodology in Section 2. Results and discussions are presented in Section 3, followed by Conclusions in Section 4.~~

2. Methodology

2.1 Brief Introduction to the Urban Atmospheric Observational Station

The Urban Atmospheric Observational Station is a regional atmospheric urban station located on the Gulou Campus of Nanjing University in the downtown area of Nanjing (32.05 °N,118.78 °E), and run by School of Atmospheric Sciences, Nanjing University. It is built on the roof of a 79.3m tall building, without any industrial pollution sources within a 30 km radius around but several main roads with evident traffic pollution, especially during rush hours. The sketch map of the site (not shown) and the corresponding climatology have been described in Zhu et al (2012).

The Particles, O_3, NO_x, NO_y (including most oxides of nitrogen mentioned above with the exception of NH_3 and N_2O), CO, and wavelength-dependent aerosol optical parameters including aerosol aerosol scattering (σ_{ts}), back-scattering (σ_{bs}), and absorption (σ_a) coefficients~~scattering (SC), back-scattering (Bsp), and absorption (AAC) coefficients~~ have been routinely measured at the station during the time period from 1 Sep 2016 to 28 Feb 2017. The σ_a ~~AAC~~ and concentrations of BC were derived from the measurements using a seven-channel Aethalometer (model AE-31, Magee Scientific, USA). The detailed calculation will be discussed below. The AE-31 model measures light attenuation (ATN) at seven wavelengths, including 370, 470, 520, 590, 660, 880 and 950 nm. The sample air is taken through a stainless-steel tube into the instruments, with a desired flow rate of 5.0 L min^{-1} and a sampling interval of 5 min during the whole period. The aerosol σ_{ts} ~~SC~~ and σ_{bs} ~~Bsp~~ were measured with a three-wavelength-integrating Nephelometer (Aurora 3000, Australia). Aurora 3000 measures aerosol light scattering, including σ_{ts} and σ_{bs} at 450, 525 and 635 nm, with a sampling interval of 1 min (Zhuang et al. 2017). The sample air was taken through a 2m stainless-steel tube with a sampling interval of 1 min, top of which is 1.5m above the roof. The inlet has a rain cap and an external as well as an internal heater to prevent condensation. In cold seasons when RH in the tube was relatively low, maximum of which was lower than 75% and most of which was lower than 50% during sunny hours, therefore the internal heater was turned off.~~The AE-31 model measures light attenuation at seven wavelengths, including 370, 470, 520, 590, 660, 880 and 950 nm, with a desired flow rate of 5.0 L min^{-1} and a sampling interval of 5 min. Aurora 3000 measures aerosol light scattering, including SC and Bsp at 450, 525 and 635 nm, with a sampling interval of 1 min (Zhuang et al. 2017).~~ $PM_{2.5}$ and PM_{10} mass concentrations were measured

using a mass analyzer (Thermo Instruments, THOM 1405-DF), which has been used to measure the mass concentration of $PM_{2.5}$, $PM_{2.5-10}$, and PM_{10} simultaneously. The hourly and daily mean mass concentrations are updated every 6 minutes, as well as the hourly base and reference mass concentrations. The sample air is taken through a stainless-steel tube into the instruments. Trace gases (CO, NO_x, NO_y and O_3) were measured every minute using online analyzers (Thermo Instruments, TEI 48i, 42i, 42iY, and 49i, respectively). Sample air was drawn from the 1.5m above the rooftop to the laboratory through a manifold connected to O_3, NO_x and CO analyzers with PFA Teflon tubes, while a separate sample line with a MoO converter was used for NO_y analyzer (Wang et al., 2002; Ding et al., 2013b) to convert other reactive nitrogen species including PAN, NO_3^- and HNO_3. Thus, the measured quantity approximates total reactive nitrogen. Precision and instrument of the measurements in this study are listed in Table 1.

Since aerosols are quite hygroscopic in China (e.g., Eichler et al., 2008; Liu et al., 2011; Ding et al., 2013b). All the instruments are installed in a laboratory with a constant temperature (24℃) and a low RH located on the building roof. Routine calibrations and maintenances were carried out for all these instruments during the sampling periods.

Monthly averaged meteorological parameters during the period from Sep.2016 to Feb.2017 at the station are shown in Table 2. The air temperature at the site ranged from 6.64℃ in Feb.2017 to 24.88℃ in Sep.2016. Both higher relative humidity (RH) and more precipitation occurred in fall than winter, especially in October. ~~The relative humidity (RH) was higher in fall than in winter, especially in October, while the precipitation was heavier in fall than in winter.~~ Visibility (Vis)

varied in different months. The peak of the ultraviolet radiation (UV) occurred in Sep.2016, after which the radiation became weak till the end of Jan.2017, and rose a little afterwards~~in Feb.2017~~.

2.2 Calculation of the aerosol optical properties

The wavelength-dependent σ_a ~~AAC~~, which is associated with the intensities of the incoming light and remaining light after passing through a medium, can be calculated directly using the measured light attenuations (ATN) through a quartz filter matrix, a percentage to represent the filter attenuation, as well as BC mass concentrations (Petzold et al., 1997; Weingartner et al., 2003; Arnott et al., 2005; Schmid et al., 2006):

~~$$\sigma_{ATN,\ t(\lambda)} = \frac{(ATN_t(\lambda) - ATN_{t\text{-}1}(\lambda))}{\Delta t} \times \frac{A}{V}$$~~

$$\sigma_{a\,ATN,\ t(\lambda)} = \frac{(ATN_t(\lambda) - ATN_{t\text{-}1}(\lambda))}{\Delta t} \times \frac{A}{V}, \quad (1)$$

where A (in m^2) is the area of the aerosol-laden filter spot, V is the volumetric sampling flow rate (in L min^{-1}) and Δt is the time interval (=5 min) between t and t-1. $\sigma_{a\,\mathrm{ATN}}$ ~~σ_{ATN}~~, known as σ_a ~~AAC~~ without any correction, is larger than the actual aerosol absorption coefficient σ_a^{abs} in general. The key factors leading to the bias are as follows: (1). multiple-scattering of light at the filter fibers (multiple-scattering effect), and (2) the instrumental response with increased particle loading on the filter (shadowing effect). The former results in the overestimation of the σ, while the later causes underestimation of the σ_a. Thus, the correction is needed and the calibration factors C and R (shown in Eq. 2) are introduced against the scattering effect and shadowing effect, respectively:

~~$\sigma_{abs,t(\lambda)}=\frac{\sigma_{ATN,t(\lambda)}}{C \times R}$,~~ $\sigma_{a\,abs,t(\lambda)}=\frac{\sigma_{a\,ATN,t(\lambda)}}{C \times R}$, (2) ~~(2)~~

~~$R_t(\lambda)=(\frac{1}{f}-1)\times\frac{\ln(ATN_t(\lambda))-\ln 10}{\ln 50-\ln 10}+1$,~~ (3) ~~(2)~~

Previous investigation suggested that wavelength-dependent σ_a corrected by Schmid (Schmid et al., 2006, SC2006 for short, hereinafter) might be the closest to the real ones in Nanjing (Collaud Coen et al., 2010; Zhuang et al., 2015). Therefore, the SC2006 is adopted in this study. In this study, the parameters in the correction procedure are derived from local optical properties (ω_0 and α_{ts} were set to 0.922 and 1.51, respectively). The values of correction factors *C* and *R* are as follows: *R*=1 when ATN≤10 and *f*=1.2, and *C* in Nanjing is 2.95, 3.37, 3.56, 3.79, 3.99, 4.51 and 4.64 at 370, 470, 520, 590, 660, 880 and 950 nm (Zhuang et al., 2015).

~~Weingartner (Weingartner et al., 2003, WC2003 for short, hereinafter), Arnott (Arnott et al., 2005), Schmid (Schmid et al., 2006, SC2006 for short, hereinafte), and Virkkula (Virkkula et al., 2007) corrections, have been developed to eliminate the uncertainties. Zhuang et al. (2015) further suggested that wavelength-dependent AACs corrected by SC2006 might be closer to the real ones than WC2003s in Nanjing, although 532 nm AACs from these two corrections are close to each other.~~

~~Therefore, AACs corrected from SC2006 are used in this study.~~

Measurement of Aurora 3000, a nephelometer with newly designed light sources based on light emitting diodes, needs correction using Mie-theory for measurement artifacts. In this study, correction was performed according to Müller et al. (2011). The raw total scattering coefficients were corrected first by calculating first the Ångström exponents from the non-corrected scattering coefficients and then following the formulas presented by Müller et al. (2011) where the tabulated

factors for no cutoff at the inlet were used, and the raw backward scattering coefficients were corrected according to the correction factors for no cutoff. And based on corrected wavelength-dependent σ_a and σ_{ts}, α_{ts} and α_a at 550 nm are estimated by the following:

$$\alpha_{a,470/660nm} = -\log(\sigma_{a,470nm}/\sigma_{a,660nm})/\log(470/660), \quad (4)$$

$$\alpha_{ts,450/635nm} = -\log(\sigma_{ts,450nm}/\sigma_{ts,635nm})/\log(450/635), \quad (5)$$

Meanwhile, aerosol asymmetry parameter (g), single-scattering albedo (ω_0) and extinction coefficient (σ_e) are further estimated:

$$\omega_0 = \frac{\sigma_{ts}}{\sigma_{ts}+\sigma_a}, \quad (6)$$

$$\sigma_e = \sigma_{ts} + \sigma_a, \quad (7)$$

~~Measurement of Aurora 3000, a nephelometer with newly designed light sources based on light emitting diodes, needs correction using Mie-theory for measurement artefacts. Müller et al. (2011) provided parameterizations for the angular sensitivity functions of Aurora 3000, which follows the definition of correction factors from Anderson and Ogren (1998), where the ratios of true to measured nephelometer values for both total scattering and backscattering are defined by:~~

~~$$C_{ts,\lambda} = \frac{\sigma_{ts,\lambda}^{true}}{\sigma_{ts,\lambda}^{neph}} \frac{\sigma_{tsR,\lambda}^{neph}}{\sigma_{tsR,\lambda}^{true}}, \quad (4)$$~~

~~and~~

~~$$C_{ts,\lambda} = \frac{\sigma_{bs,\lambda}^{true}}{\sigma_{bs,\lambda}^{neph}} \frac{\sigma_{bsR,\lambda}^{neph}}{\sigma_{bsR,\lambda}^{true}}, \quad (5)$$~~

~~where σ_{ts}^{true} and σ_{bs}^{true} are true total scattering coefficient and backscattering coefficient for ideal~~

angular sensitivity functions, respectively, $\sigma_{tsR,\lambda}$ and $\sigma_{bsR,\lambda}$ are Rayleigh total scattering coefficient and backscattering coefficient, respectively, and σ_{ts}^{neph} and σ_{bs}^{neph} are nephelometer total scattering coefficient and backscattering coefficient, respectively. In this study, we assume that Rayleigh scattering is equivalent to true scattering.

The correction factors can be calculated using measured size distributions or SAE. Anderson and Ogren (1998), hereinafter denoted as AO98, found a dependency between the SAE and the correction factor for total scattering. The correction was given by:

$$C_{ts} = a + b \cdot \alpha_{ts}^{*} \quad (6)$$

where α_{ts}^{*} is the scattering Ångström exponent derived from uncorrected nephelometer scattering. According to Müller et al. (2011), for backscattering, there was no correlation between correction factors and scattering Ångström exponents, which is in agreement with AO98. The parameters a and b were derived from Mie calculated true scattering and simulated nephelometer scattering for ranges of particle sizes and refractive indices.

In this study, we used the correction factors for Aurora 3000 without a sub-μm cut in Müller et al. (2011), which are shown in the Table 3. According to nephelometer correction factors for angular nonidealities, which are shown in Table 3(a), original scattering coefficient (SC at 635 nm, 525 nm and 450 nm) and backscattering coefficient (Bsp at 635 nm, 525 nm and 450 nm) obtained from the measurements are corrected based on Eqs (4) and Eqs (5). We also calculated correction factors for total scatter as function of Ångström exponent shown in Table 3.(b), original scattering coefficient (SC at 635 nm, 525 nm and 450 nm) are corrected based on Eqs (6).

Based on corrected wavelength-dependent AAC and SC, SAE and AAE are estimated by the following:

$$AAE_{470/660nm} = -\log(AAC_{470nm}/AAC_{660nm})/\log(470/660), \quad (7)$$

$$SAE_{450/635nm} = -\log(SC_{450nm}/SC_{635nm})/\log(450/635), \quad (8)$$

$$\sigma_{\lambda} = \sigma_{\lambda_0} \times (\frac{\lambda}{\lambda_0})^{-\alpha}, \quad (9)$$

where σ_{λ} is the coefficient at wavelength λ and α is the corresponding Ångström exponents.

On the basis of Eqs (7) ~ Eqs (9), SC and Bsp at 550 nm were calculated for comparison. Between the two ways of corrections, the results of the total scattering coefficients are in agreement with each other in general, with differences of 10.67%. In this study, we choose the results from the correction using SAE.

Meanwhile, based on wavelength-dependent SC, Bsp, AAC, aerosol asymmetry parameter (ASP), single-scattering albedo (SSA) and extinction coefficient (EC) are further estimated:

$$ASP_{\lambda} = -7.143889\beta_{\lambda}^{3} + 7.46443\beta_{\lambda}^{2} - 3.9356\beta_{\lambda} + 0.9893, \quad (10)$$

$$SSA_{\lambda} = \frac{SC_{\lambda}}{SC_{\lambda} + AAC_{\lambda}}, \quad (11)$$

$$EC_{\lambda} = SC_{\lambda} + AAC_{\lambda}, \quad (12)$$

where is β_{λ} the ratio of Bsp to SC at wavelength λ. Equation (10) is derived from Andrews et al. (2006).

Table 4 shows the statistical summary of the surface aerosol optical properties in Nanjing after the correction. The mean value during the cold seasons in 2016 of AAC, SC, Bsp, EC, SSA and ASP at 550 nm, AAE at 470/660 nm and SAE at 450/635 nm are 23.741, 349.502, 35.469, 373.536 Mm^{-}

~~^{1}, 0.929, 0.645, 1.600, and 1.192, with a standard deviation of 15.556, 235.291, 21.488, 247.877~~

~~Mm^{-1}, 0.028, 0.052, 0.175, and 0.288, respectively.~~

2.3 HYSPLIT model

In order to understand the general transport characteristics of air masses recorded at this station, we conducted a 4 d (96 h) backward trajectory simulations during the cold seasons in 2016 using a Lagrangian dispersion model Hybrid Single-Particle Lagrangian Integrated Trajectory (HYSPLIT) (version 4.9) provided by the Air Resource Laboratory (ARL) of the USA National Oceanic and Atmospheric Administration (NOAA) (Draxler and Hess, 1998). HYSPLIT - 4 Model is capable of processing multiple gas input fields, multiple physical processes and different types of pollutant emission sources and has been widely used in the study of transport and diffusion of various pollutants in various regions (Mcgowan and Clark, 2008; Wang et al., 2011; Wang et al., 2015). It is one of the most extensively used atmospheric transport and dispersion models for the study of air parcel trajectories (Draxler and Rolph, 2013; Stein et al., 2016). In this study, backward trajectories were calculated and clustered using a stand-alone version of the GDAS (Ground Data Acquisition System) meteorological field (ftp://arlftp.arlhq.noaa.gov/pub/archives/gdas1)~~the NCEP / NCAR reanalyzed meteorological field (http://ready.arl.noaa.gov/archives.php).~~ The ~~NCEP~~ GDAS data contains 6-hourly basic meteorological fields on pressure surfaces, with the spatial resolution of ~~2.5~~1.0°, corresponding to the 00, 06, 12, 18 UTC, respectively. In this study, the data are also converted to hemispheric 144 by 73 polar stereographic grids, which is the same grid configuration as the dataset applied in synoptic weather classification. For each synoptic weather pattern, the

backward trajectories were started at Gulou station in Nanjing (32°N, 118.8°E).

3. Results and discussion

3.1 Characteristics of particulate matter in Nanjing

The hourly-mean concentrations of particles at Gulou site during the cold seasons in 2016 are shown in Fig 1. Gaps in the time series are missing values.

Observations show that peaks and valleys of BC, $PM_{2.5}$ and PM_{10} occur simultaneously in general (Fig 1a), probably because the three particles originate mostly from the same sources, i.e., fossil fuel burning and traffic activities. It has also been addressed in previous work (e.g., Wang et al., 2008; Chow et al., 2011; Schleicher et al., 2013; Zhuang et al., 2014b; Gong et al., 2015).

~~The averaged values of BC, $PM_{2.5}$ and PM_{10} during the study period are 2.6±1.7, 58.2±36.8, and 86.3±50.8 μg/m³, respectively. The average of particulate matter concentrations during the study period are higher than standard concentrations, which are 35 μg/m³ for fine and 70 μg/m³ for PM_{10}. Particles, including BC, $PM_{2.5}$ and PM_{10} fluctuate similarly, because the three particules originate mostly from the same sources, i.e., transport emissions. BC loadings at Gulou were low in September and October, usually below 6 μg/m³, while the loadings were high in the other months, such as in mid-November, early and late December, early January, and mid-to-late February, suggesting occurrences of BC pollution events during these periods. $PM_{2.5}$ loadings and PM_{10} loadings were generally below 120 and 200 μg/m³, respectively, but higher during early October and in the periods when BC loadings were high. The particle concentrations are affected by various factors and progress. For example, the high loadings of particulate matter in early October was mainly due to the increase in aerosols concentrations with high scatter coefficient (SC), and thus the~~

~~BC loadings did not show such peak during early October.~~

BC concentration ranged from 0.064 to 15.609 μg/m³. Seasonal mean of BC concentration was 2.126 μg/m³ in SON and 3.083 μg/m³ in DJF, with a standard deviation of 1.457 and 1.827 μg/m³, respectively. It was low in September and October, usually below 6 μg/m³, but higher in other months. Although BC concentration was relatively low, it was extremely high in particular periods, , such as in mid-November, early and late December, early January, and mid-to-late February, suggesting occurrences of substantial BC pollution events. $PM_{2.5}$ and PM_{10} concentration ranged from 0.8 to 256.4 μg/m³ and from 1.1 to 343.4 μg/m³, respectively. Seasonal mean of $PM_{2.5}$ concentration was 43.1 μg/m³ in SON and 73.2 μg/m³ in DJF, with a standard deviation of 25.4 and 40.0 μg/m³, respectively. PM_{10} averaged 67.6 μg/m³ in SON and 105.0 μg/m³ in DJF, with a standard deviation of 39.1 and 54.0 μg/m³, respectively. $PM_{2.5}$ and PM_{10} concentration were generally below 120 and 200 μg/m³, respectively. Remarkable increases existed especially when BC concentration was high. Additionally, the high concentrations of PMs in early October possibly resulted from the increase in scattering aerosols, since absorption coefficient and BC, one of typical absorbing aerosols, did not show such peak, while scatter coefficient experienced a sharp increase during that period. It is found that both BC and PMs levels in Nanjing became lower compared to those in earlier years, which is possibly due to the strengthening energy conservation and reduction of pollution emissions from 2014. For instance, seasonal average in SON and DJF were reported 4339 and 4189 ng/m^3 in urban Nanjing during 2012 in Zhuang et al. (2014b), and Ding et al. (2013b) stated a 1-year average about 75 μg/m^3 of $PM_{2.5}$ in rural area of Nanjing form August 2011 to July 2012, while Wang et al. (2014) suggested that annual average of $PM_{2.5}$ and PM_{10} were 75 and 135

μg/m^3 in Nanjing during 2013, respectively.

Monthly variations of particles in the cold seasons in 2016 were obvious (Fig.2). The concentrations increased from October to December and decreased a little afterwards but remained relatively high in January and February. ~~High particle concentrations were observed from November to February while the low ones were in September and October.~~ The lowest~~smallest~~ monthly concentrations of BC, $PM_{2.5}$, and PM_{10} occurred in October, being 1.8, 39.2, and 59.8 μg/m³, respectively, while the largest monthly concentrations occurred in December, being 3.7, 85.0, and 123.1 μg/m³, respectively, which were about twice of those in October. Monthly variations of BC were different from those in previous studies in YRD. For instance, Pan et al. (2011) pointed out an extremely high concentration in October in Mt. Huang, which was attributed to combustion of biomasses as well as the dynamic transport and stable planetary boundary layer (PBL) stratification in the transitional periods of the winter monsoon (October). For PMs, monthly behavior was basically similar to what has been reported in previous studies in YRD, increasing from September to December in general (Chen et al., 2016), except the decrease in October. ~~In general~~Generally, ~~there are~~ two key factors ~~that~~ could impact particle concentrations: meteorology and emissions. Heavy precipitation ~~with a strong scavenging effect~~ in October when average rainfall was 3.1 mm, and the frequency of daily rainfall exceeding 50mm was over 30%~~might directly lead to small loadings of particles~~ (Table.2), had a strong scavenging effect, which might directly lead to low levels of particles despite the influence of biomass burning addressed in Pan et al. (2011).~~.~~ Anthropogenic particle emissions from fossil fuel over China increased after summer and showed a sharp increase from November to January (Zhang et al., 2009), , and emission rates in southwest (Sichuan basin), central to north, and

northeast China, as well as YRD and PRD were higher in winter (Zhuang et al., 2018), especially in residential, industry and power emissions (Li et al., 2017)~~which may explain the high particle concentrations during those periods~~. And during the autumn harvest (September~ November), though not so much as that in summer, the crop burning emissions in still make contribution to pollutants (Yang et al., 2008). Yin et al. (2016) discussed the spatial distribution of crop residue burning from September to December in 2015, suggesting autumn crop residue burning in surrounding regions like Shandong, Anhui and Henan Provinces, thus, particles in Nanjing might also be subject to these large-scale burning of crop residues (Qian et al., 2014). According to Huang et al. (2012) and Li et al. (2016), spatiotemporal distribution of agricultural fire occurrences in China during 2003~ 2010 as well as 2012 has been presented associated with the spatial distribution of CO emission from residue open burning. Both of them suggested the crop residue burning in autumn is noteworthy and Jiangsu as well as the surrounding provinces are the regions with highest emissions. Besides, sub-regional transport also plays an important role, for example, in winter, air masses coming from North China Plain, which accounts for 31%, have high particles concentrations (Sect 3.4).

~~Qian et.al (2014) believed that high particle loadings in Nanjing from late October to early November resulted from the large-scale burning of crop residues. However, $PM_{2.5}$ and PM_{10} concentrations reached a relative maximal in early October, while the emission in October is relative low compared to the following months (Zhang et al., 2009).~~

Substantial diurnal cycles of the particles are also observed (Fig.3). Particles levels were high during 7:00~9:00 and 22:00~0:00 LT but low in afternoon (13:00~15:00 LT).~~BC levels were high at rush~~

~~hours (7~9 am and 8~11 pm) but low in afternoon (1~3 pm).~~ High concentrations during 7:00~9:00 LT ~~Zhuang et al. (2014) mentioned that high BC concentrations in these times of the day~~ might be caused by the vehicle emissions (as mentioned in Section 2, several main roads with apparent traffic pollution surround the station). A higher vehicle volume showed during 17:00~ 20:00 LT in Nanjing, while the high concentrations occurred during 22:00~ 0:00 LT. A lower temperature and a more stable atmosphere stratification after sunset (17:00~18:00 LT) often lead to frequent temperature inversion and low height of planetary boundary layer (Jiang et al., 2014), which is not conductive to the diffusion of pollutants, and the concentrations of particles accumulate and remain high from the evening to early morning. ~~In addition, temperature was low after midnight, and the atmosphere stratification was stable. Therefore, it was easy for temperature inversion to appear, which was not conductive to the diffusion of pollutants, and the concentrations of particles accumulated and reached a peak at around 8 am. Atmosphere stratification became stable again as the temperature decreased after around 4 pm, which may also explain the peak during 9~11 pm (Qian et al., 2014).~~ For low levels in afternoon, it is mainly induced by well-developed boundary layer. Because the atmosphere become less stable with the increasing temperature, and strong turbulent exchange as well as vertical diffusion are favorable to the diffusion of pollutants, particles concentrations decrease to a minimum in the afternoon. ~~As to the low BC in afternoon, which occurred at around 3 pm, it was mainly induced by well-developed boundary layer. Because the atmosphere became less stable with increasing temperature, and strong turbulent exchange and vertical diffusion were favorable to the diffusion of pollutants, BC concentrations decreased to a minimum in the afternoon.~~ Similar phenomenon of PMs has been observed in previous studies in Nanjing (Chen et al., 2016; Ding et al., 2013b), while a different pattern is discussed in Pan et al. (2011) in Mt. Huang, a rural

site in YRD, due to different emission sources (less vehicle emission) and meteorology effects (effect of valley breezing). Fig. 3 also shows that the peak values of fine particle concentrations often occurred ~~one or two hours~~1~ 2 h later than those of BC concentrations, with high values at around 10~~ am~~:00 and low values at around ~~5 pm~~17:00 LT. According to Roberts and Friedlander (1976) and Khoder (2002), atmospheric photochemical reactions are extremely active under conditions of strong radiation and high temperature, especially during daytime, thus, ~~during which more secondary aerosol particles (like sulfate particles) generated, so~~ more secondary aerosol particles (like sulfate particles) are likely to generate, and the concentrations of fine particles in the atmosphere will increase.~~ When solar radiation was strong, ultra-fine particles generated during photochemical reactions contributed greatly to the concentrations of aerosol particles~~.

~~Generally, the diurnal cycles of BC had a bimodal distribution with two peaks, while $PM_{2.5}$ and PM_{10} had only one peak. However, both magnitude and temporal variations of particles were changed in winter, and there is another peak at around 2 am（see S1）, which was possibly due to the affection of BC pollution episodes at night.~~

3.2 Characteristics of gaseous pollutants in Nanjing

Fig.4 shows hourly-mean concentrations of gaseous pollutants at Gulou during the cold seasons in 2016~~, in which, there were few gaps for invalid values~~. In general, as main precursors of O_3, NO_x, NO_y, and CO generally show different pattern with O_3, such as when the precursors levels remained high from November to January, O_3 levels were relatively low (Xie et al., 2016; Wang et al., 2017). Also, the precursors concentrations varied greatly, especially in DJF (with several peaks), possibly

because of the frequent shifting of air masses from the clean interior continent and heavily polluted urban plumes in the heating period (normally from November to March in Northern China) (Pan et al., 2011).

Concentrations of trace gases, including CO (176~ 2852 ppb), NO_x (2.7~ 80.0 ppb), NO_y (3.6~ 158.4 ppb), and O_3 (0.2~ 235.7 ppb), varied a lot in the study period. Seasonal mean of O_3 was 42.3 ppb in SON and 33.1 ppb in DJF, with a standard deviation of 40.1 and 24.4 ppb, respectively. ~~The averaged concentrations during the fall and winter of CO, O_3, NO_x and NO_y at the site are 851 ± 384, 37.7 ± 33.5, 23.5 ± 14.7, and 32.8 ± 22.3 ppb, respectively.~~ As shown in Fig.4, O_3 concentrations ~~in the site were~~ was extremely high during the ~~entire~~ whole September in 2016, with a maximum over 200 ppb,– and decreased sharply after mid-October, basically keeping a low level below 100 ppb, until early February when it began to increase. ~~which was mainly due to the strong solar radiation and the high temperature lasting in September. O_3 concentrations began to increase in February because of enhanced solar radiation, after a low-concentration period since late October, during which O_3 concentrations were below 100 ppb.~~ Seasonal averages of NO_x and NO_y, were 21.4 and 28.6ppb in SON, with a deviation of 20.5, and 40.1 ppb, respectively. In DJF, mean concentrations of NO_x and NO_y were 27.6 and 37.0 ppb, with a deviation of 15.5 and 23.1 ppb. And seasonal averages of CO were 753 ppb in SON, and 950 ppb in DJF, with a deviation of 353 and 388 ppb, respectively. The precursors concentrations were high from November to mid-January, and low in September~~NO_x and NO_y have a similar pattern: the concentrations were high in November, December and February (Fig.5)~~. Moreover, it is suggested that O_3 concentration is higher compared to the results in previous studies in Nanjing (Xie et al., 2016; An et al., 2015; Ding et al., 2013b), implying a more pressing environmental issue of near-surface O_3 problem in urban

area.

~~It is noticeable that the daily variation of CO concentrations was similar to that of BC. A remarkable correlation between BC and CO is found in a number of studies (Jennings et al., 1996; Derwent et al., 2001; Badarinath et al., 2007; Spackman et al., 2008), suggesting that both of the pollutants are greatly affected by anthropogenic sources and biomass burning in eastern China.~~

Monthly variations of trace gases are shown in Fig.5. ~~Fig.5 illustrates monthly variations of O_3, nitrogen oxides (NO_y and NO_x), and CO in the cold seasons in 2016.~~ It is noticeable that the different patterns occur in O_3 and its precursors. Observations show that O_3 concentration decreased after the lasting extremely high level in September until November and increased a little afterwards. Highest concentration of O_3 was found in September and lowest in November, being 74.8 and 23.4 ppb, respectively. This pattern might be attributed to the solar radiation and emissions. For instance, in September when solar radiation was strong (maximum UV over 55 W/m^2), it would contribute greatly to O_3 formation, and precursors were at relatively high levels (CO, NO_x, and NO_y were about 600, 15 and 20 ppb, respectively), though not as high as those in cold days. CO, NO_x and NO_y peaked in December correspondingly at 1064, 31.8 and 41.7 ppb. The precursors reached the lowest level in September, being 620, 14.5, and 20.8 ppb, respectively. In addition, the pattern of precursors is analogous to those in previous studies (Xie et al., 2016; Ding et al., 2013b), but with a relatively lower concentration, especially NO_x and NO_y, which might also result from the large-scale reduction of pollution emissions.

~~O_3 peaked in September at 74.8 ppb while NO_y and NO_x peaked in December at 31.8 and 41.7 ppb, respectively. O_3 reached minimum at 23.4 ppb in November and NO_y and NO_x ware lowest in~~

September, being 14.5, and 20.8 ppb, respectively. O_3 is a secondary pollutant and complicatedly related to its precursors, including NO_x and VOCs. O_3 precursors and their effects on O_3 formation are different at different geographical locations, and thus the characterizations of O_3 at different sites can vary greatly. O_3–NO_x–VOCs relationships can be described by the following reactions:

$O(^3P) + O_2 + M \rightarrow O_3 + M$ (R1)

$NO_2 + h\upsilon \rightarrow NO + O(^3P)$ (R2)

$O_3 + NO \rightarrow O_2 + NO_2$ (R3)

$HO_2 + NO \rightarrow OH + NO_2$ (R4)

$RO_2 + NO \rightarrow OH + NO_2$ (R5)

$OH + RH + O_2 \rightarrow RO_2 + H_2O$ (R6)

$RO + O_2 \rightarrow HO_2 +$ carbonyls (R7)

where (R4), (R5), and (R2) reactions establish an "NO_X cycle" that could produce O_3 without consumption of NO_X, the other important chemistry cycle is the so-called "RO_X (RO_X=OH+HO_2 + RO_2) radical cycle" that could continuously supply HO_2 and RO_2 to oxidize NO to NO_2, and (R7) is usually referred as NO_x titration, which is an important O_3 removal process related to freshly emitted NO. In general, when NO_x concentrations were high, O_3 concentrations may experience a depression process since excessive NO are not favorable for the O_3 production (Xie et al, 2016; Wang et al., 2018). The CO concentrations varied greatly in winter because of the frequent shifting of air masses from the clean interior continent and heavily polluted urban plumes in the heating period (normally from November to March in Northern China, (Pan et al., 2011). In September and October, the CO concentrations at Gulou apparently decreased owing to frequent intrusions of clean air mass from the Pacific Ocean, and this seasonal trend was confirmed by HYSPLIT-4 model (see

~~detailed discussion in Section.4).~~

Fig. 6 (a) shows the ~~mean~~ diurnal variations of the gaseous pollutants (O_3, NO_x, NO_y, and CO) ~~at Gulou during the cold seasons in 2016~~. The concentration~~s~~ of O_3 ~~were~~ is the lowest around 7:00 LT~~7 am~~ and rises rapidly until reaching the peak in the middle of the day at 15:00 LT. ~~went up rapidly corresponding with the increase of solar radiation. After reaching the peak in the middle of the day at 3 pm,~~ It keeps decreasing sharply after the afternoon peak till sunset. During the nighttime, the concentration of O_3 decreases slowly and remains low. ~~the O_3 concentrations kept decreasing rapidly until sunset. During the nighttime, the concentrations of O_3 decreased slowly and maintained low values, attributed to the process of NO_x titration and the lack of solar radiation.~~ With respect to NO_x and NO_y, peak appears at around 9:00 LT, with another high value occurring at night (21:00~0:00 LT), both of which coincide with the rush hours in the city, when ~~two peaks appeared in the diurnal cycles, one around 9 am and the other at 8 pm. Both peaks coincided with the rush hours in the city, during which~~ large amounts of vehicle emissions ~~were~~ are released. The morning peak is~~was~~ slightly higher than the ~~evening~~ night one in general. ~~Besides emissions, According to Xie et al. (2016),~~ these diurnal variation patterns of O_3 and NO_x ~~are~~ mainly result~~ed~~ from the photochemical processes and the meteorological conditions. Simultaneous measurement of O_3 and UV shows that the O_3 concentration is highly correlated to UV (R=0.71, Fig. 9(a)). The ultraviolet irradiance (UV) at Gulou start~~sed~~ to increase at about 7~~ am~~:00 LT (Fig.6 (b)), which could induce a series of photochemical reactions including the formation of peroxy radicals (HO_2 and RO_2 etc.) and the photolysis of NO_2. From 8~~ am~~:00 to ~~3 pm~~15:00 LT, the increase in UV ~~enhanced~~ enhances the O_3 formation by promoting the production processes of NO_2 and OH from NO and peroxy

radicals~~(R4) (R5)~~. ~~Simultaneous measurement of O_3 and UV shows that the O_3 concentrations are highly correlated to UV, with a correlation coefficient of 0.47.~~ The diurnal range of O_3 concentration (the difference between the maximum at 15:00 LT and the minimum at 7:00 LT) is relatively high (45.1 ppb), suggesting the active chemical reactions as well. It is also noticeable that ~~the~~ O_3 peaks ~~maximum was~~ 2 h after the UV maximum, suggesting the time to take for the chemical reactions. The slightly reduction of O_3 and NO_x ~~after the midnight~~in the early morning (3:00~7:00 LT) is likely due to ~~of~~ NO_x titration. The development of the planetary boundary layer (PBL) can also modulate pollutant concentrations. The concentration~~s~~ of a pollutant ~~are~~ is diluted when PBL rise~~s~~ during the daytime and enhanced in the low nocturnal PBL that favors pollutant accumulation, after comparing Fig.6 (a) with the reported diurnal variation of PBL height in Nanjing (Jiang et al., 2014; Xie et al., 2016). And that is also the reason for the difference of peak time between the emission rate and NO_x (NO_y) concentration, which is similar to particles to some degree. The abovementioned diurnal cycles in O_3 and NO_x (NO_y) concentrations follow the typical patterns at other sites in Nanjing (Tu et al., 2007; Ding et al., 2013b; Xie et al, 2016). The daily variation of CO concentration is found to be similar to that of BC, such as morning peak during rush hours, afternoon dip at around 15:00 LT, and accumulation at night. A remarkable correlation has been found in a number of previous studies (e.g., Jennings et al., 1996; Derwent et al., 2001; Badarinath et al., 2007; Spackman et al., 2008; Pan et al., 2011; Zhuang et al., 2014b). Besides, BC is mostly produced by the incomplete combustion of carbonaceous material, and so is carbon monoxide (CO) (Pan et al., 2011), thus, both BC and CO might come from the same sources, mostly from combustions of domestic bio-fuel, industry-coal, and vehicle-gasoline (Zhuang et al., 2014b). The effect of meteorology, i.e., the development of PBL, influences the diurnal pattern as mentioned in Section 3.1, especially the

afternoon dip and night accumulation. Moreover, as one of main precursors of O_3, increase in O_3 levels in the afternoon might also contribute to the lowest concentration at 15:00 LT.

Table ~~7~~ 5 further provides the statistics of O_3, $PM_{2.5}$ and PM_{10} mass concentrations with a comparison to the National Ambient Air Quality Standards in China (NAAQS-CN), which were released in 2012 by the China State Council and will be implemented nationwide in 2016 (MEP, 2012). According to NAAQS-CN for $PM_{2.5}$ and PM_{10} (75 μg/m^3 of $PM_{2.5}$ concentrations and 150 μg/m^3 of PM_{10} concentrations for 24h average), there were 48 days of $PM_{2.5}$ exceedances, accounting for about 30% of the 6 months period, and 14 days of PM_{10} exceedances, lower than the $PM_{2.5}$ exceedances. Days of ~~particulate matter~~PMs exceedances mainly occurred during DJF. The days of exceedances decreased. ~~Donkelaar et al. (2010) reported that a multi-year average of $PM_{2.5}$ mass concentrations was over 80 μg/m^3 in eastern China by using satellite data during 2001–2006, and~~ Ding et al. (2013b) ~~stated~~reported 99 days of $PM_{2.5}$ exceedances in total from September 2011 to February 2012, and Wang et al. (2014) suggested that non-attainment rates in Nanjing from September 2013 to February 2014 were over 40% and 70% in SON and DJF, respectively. ~~an 1-year average about 75 μg/m^3 in rural area of Nanjing form August 2011 to July 2012. Therefore, the means in Table 7 show lower particle concentrations than what were reported. The days of exceedances also were fewer than in 2011 (Ding et al., 2013), during which 99 days of $PM_{2.5}$ exceedances happened during the cold seasons.~~ These results suggest that particles control policies are well-implemented in Nanjing although particles remain a severe pollution problem in the YRD region. According to NAAQS-CN for O_3 (160 μg/m^3 for 8 h average and 200 μg/m^3 for 1 h average), 37 days of exceedances occurred (~~Table7~~Table 5), covering 20% of the period and mostly appearing

in September and February when the air temperature was relatively high. In contrast to particulate matter, days of O_3 exceedances increases greatly. ~~O_3 concentrations increased from 2011 to 2016, and the exceedance days were 10 times of those in 2011.~~ Wang et al. (2014) reported a 11.4% contribution of O_3 as the major pollutant on non-attainment days in cold seasons in 2013 in south-east China, and Tu et al. (2007) reported frequency of days with O_3 exceedance for cold seasons in 2000~2002 in urban Nanjing was 6.3%. ~~It was found in previous studies that~~ O_3 levels in the rural areas ~~were~~ are generally higher than those in the city centers (Zhang et al., 2008; Geng et al., 2008; Xie et al., 2016). Thus, high O_3 concentrations and severe air pollution in Gulou, an urban site, probably ~~suggest~~ imply a severer O_3 pollution problem in the entire YRD region. Moreover, ~~N~~note that this study only discussed the O_3 concentration~~s~~ in the cold seasons when ~~the concentrations of O_3 are lower than in the warm season~~it is relatively low, and it might suggest ~~the problem can be~~a severer problem in the warm seasons. ~~The emissions of O_3 precursors (VOCs and NO_y) in Nanjing have significantly increased with the increases of residents (over 200,000 increase since 2011), the number of automobiles (over 65% increase since 2011), and GDP (gross domestic production) (nearly 70% increase since 2011). Consequently, O_3 concentrations at ground level has gradually risen (http://www.njtj.gov.cn/).~~

3.3 Inter-species correlations

Correlations between different species ~~were~~ have been analyzed to help interpret the data and gain insights into the underlying mechanisms/processes. Because precipitation could impact wet scavenging processes for particles and other aerosols (~~see S2~~Table 6), the data in rainy condition

has been eliminated. ~~we eliminated the data in rainy condition.~~

The scatter plot of O_3 measured at the site and NO_x color-coded with air temperature is given in Fig.7 (a). As discussed in previous studies (Xie et al., 2016; Ding et al., 2013b), measured O_3 presents an overall negative correlation with NO_x.~~The negative correlation suggests a titration effect of freshly emitted NO with O_3 in the cold seasons.~~ The negative correlation mainly exists for data of relatively low air temperature, suggesting a titration effect of freshly emitted NO_x with O_3, especially at nighttime. However, the slope gets less rigid when air temperature rises, and tend to be positive with a high temperature (over 25℃) and low level of NO_x (below 30 ppb).~~In addition, the slope decreased when air temperature rose.~~ These results possibly suggest a strong photochemical production of O_3 in this region under high temperature with strong radiation like in September ~~during high air temperature~~, leading to~~resulting in~~ the seasonal cycle pattern of O_3 shown in Fig. 5 (a) ~~(Ding et.al, 2013)~~.

Fig.7 (b) provides a scatter plot of $PM_{2.5}$ and visibility (Vis) color-coded with relative humidity (RH). ~~Previous research has shown that visibility has a good correlation with the concentrations of particles and relative humidity.~~ For a better understanding of the relationship between the variables, we have performed a linear fit of the visibility with the $PM_{2.5}$ concentration when RH ≤ 70%, 70% <RH ≤ 80%, and 80% < RH ≤ 90%, to find out the relationship among these factors, and the fitting curves are $[PM_{2.5}] = 366.72[Vis]^{-0.745}$ ($R^2 = 0.7196$), $[PM_{2.5}] = 337.16[Vis]^{-0.855}$ ($R^2 = 0.8692$), and $[PM_{2.5}] = 248.6[Vis]^{-0.852}$ ($R^2 = 0.8279$), respectively. It is found that visibility decreases with the concentration of $PM_{2.5}$ in a power function with a negative exponent, and the inverse relationship

between visibility and aerosols concentrations as well as relative humidity has also been discussed in previous studies based on the observations in YRD (e.g., Deng et al., 2011; Xiao et al., 2011; Jiang et al., 2018). The correlation is stronger than that in Lin'an, a rural site not far from Nanjing (Jiang et al., 2018). ~~With an increase in the $PM_{2.5}$ concentrations, visibility decreases exponentially (Fig.7 (b)), because t~~The concentrations of particles would increase scattered and absorption extinction coefficients, while the visibility (Vis) is related to the coefficients through:

$$Vis = \frac{3.91}{\sigma} \quad (\text{~~1~~}38)$$

where Vis is the visibility and σ is the extinction coefficient (EC) (Larson et.al, 1989). As for the effect of relative humidity (RH) on the visibility, according to Mie theory, with the increase of the relative humidity, the radius of the wet particle also increases, and so does the extinction coefficient, which leads to the decrease in visibility ~~increases~~. ~~Therefore, the visibility decrease. Moreover, when RH≤ 80%, the effect of particle concentrations on visibility could become smog, and when 80% < RH ≤ 90%, the effect could form smog and fog at the same time. Thus, we performed a linear fit of the visibility with differing concentrations of $PM_{2.5}$ when RH ≤ 70%, 70% <RH ≤ 80%, and 80% < RH ≤ 90%, to find out the relationship among these factors. Although there is no precipitation, there are still water droplets in the air when RH >90%, which become fog. Therefore, we eliminated those data. It is found that the fitting curves are as follows: $[PM_{2.5}] = 366.72[Vis]^{-0.745}$ ($R^2 = 0.7196$), $[PM_{2.5}] = 337.16[Vis]^{-0.855}$ ($R^2 = 0.8692$), and $[PM_{2.5}] = 248.6[Vis]^{-0.852}$ ($R^2 = 0.8279$).~~

According to the scatter plots of $PM_{2.5}$–O_3 and BC–O_3 color-coded with air temperature (Fig.8), $PM_{2.5}$ and BC are negatively correlated with O_3 in general. ~~To figure out the interaction between particles and O_3, we give scatter plots of $PM_{2.5}$–O_3 and BC–O_3 (Fig.8), in which data points are~~

~~color-coded with air temperature. Overall, particulate matters and black carbon are negatively correlated with O_3.~~ It is also noticeable that a negative correlation between $PM_{2.5}$ and O_3 could be found for low air temperature samples while a positive correlation exists for those under a high temperature. Similar results were also found at a rural site in Nanjing (Ding et al., 2013b). Besides, BC is in a negative correlation with O_3 under low air temperature, but tend less-correlated with O_3 when the temperature rises. $PM_{2.5}$ is well-correlated with O_3 precursors, such as NO_x (Fig.10 (b)) and CO. Therefore, the anti-correlation in Fig.8 (a) for cold air is likely due to the titration effect of high NO concentrations associated with high primary $PM_{2.5}$ levels. ~~And~~Additionally, the increasing slope under ~~the positive correlation for~~ high air temperature ~~is~~might be related to the formation of secondary fine particles ~~associated with high concentrations of O_3, which may be related to~~especially the high conversion rate of SO_2 to sulfate under the effect of high concentrations of oxidants (~~Khoder, 2002~~O_3) and solar radiation (Roberts and Friedlander, 1976; Khoder, 2002). Previous studies of $PM_{2.5}$ chemical compositions in Shanghai ~~and Nanjing~~ (Wang et al., ~~2002,~~ 2006) and Nanjing (Ding et al., 2013b) suggested that sulfate was the most dominate ion in $PM_{2.5}$. Ding et al. (2013b) also suggested formation of secondary organic aerosols with high O_3 concentration could lead to the positive correlation because biogenic emission of VOCs is high under a condition of high air temperature and solar radiation in summer. However, the study is performed during cold seasons when air temperature is relatively lower and the biogenic emission of VOCs are likely lower, so the positive correlation is less pronounced. As for BC, it also shows a good correlation with NO_x (Fig.10 (c)) and CO, which contributes to the inverse correlation for cold air. Since ~~black carbon~~BC is insoluble in polar and non-polar solvents and remains stable when air or oxygen is heated to 350 ~ 400°C, it's hard ~~it cannot~~ to be generated ~~n~~or cleared through chemical reactions. And that is

probably the reason why~~Thus, when air temperature rises,~~ the correlation between BC and O_3 ~~becomes~~is obscurer compared to the one between $PM_{2.5}$ and O_3 when air temperature rises. Moreover, as shown in Fig.9, O_3 is well correlated with UV (daily averages are used due to the remarkable diurnal variation), suggesting the significant role UV plays in O_3 production, while $PM_{2.5}$ is generally negatively correlated with UV. Previous findings based on various numerical models also suggest that particles can affect actinic flux of UV radiation, and inhibit the photolysis reactions near surface in reducing the photolysis frequencies in the atmosphere, like the frequency of $O_3 \rightarrow O(^1D)$ (e.g., Li et al., 2005; Deng et al., 2010; Li et al., 2011; Li et al., 2018). In central Nanjing, as implied in Li et al. (2017), high concentrations of aerosols could result in a 0.1−5.0 ppb (12.0%) reduction of near-surface O_3. Thus, they might result in the decrease of O_3 concentration near the ground to some degree. ~~because particulates inhibit the photolysis reactions near the surface, reducing the photolysis frequencies in the atmosphere, and resulting in the decrease of O_3 concentrations near the ground, which is also addressed using the chemical transport model (HANK) (Li et al., 2005). It is noticeable that a negative correlation could be found for low air temperature samples while a pronounced positive correlation existed for high temperature data points. The negative correlation for cold air is mainly due to the titration effect of high NO concentrations, which was associated with high primary $PM_{2.5}$ in the cold seasons as well. And the positive correlation for high air temperature is related to the formation of secondary fine particles associated with high concentrations of O_3, which may be related to high conversion rate of SO_2 to sulfate under high concentrations of oxidants (Khoder, 2002). Previous studies of $PM_{2.5}$ chemical compositions in Shanghai and Nanjing (Wang et al., 2002, 2006) suggested that sulfate was the most dominate ion in $PM_{2.5}$.~~ However, ~~T~~the detailed mechanisms still need to be further investigated~~addressed~~ by

long-term measurement of aerosol chemical composition combined with numerical models. ~~Since black carbon is insoluble in polar and non-polar solvents and remains stable when air or oxygen is heated to 350 ~ 400°C, it cannot be generated nor cleared through chemical reactions. Thus, when air temperature rises, the correlation between BC and O_3 becomes obscurer compared to the one between $PM_{2.5}$ and O_3.~~

Scatter plots of CO–NO_x, $PM_{2.5}$–NO_x, and BC–NO_x, are given in Figs. ~~9~~10 (a)~~ ~~9~~(c), with data points color-coded with concentrations of O_3. Fig.~~9~~ 10 (b) and ~~9~~(c) show a good positive correlation between $PM_{2.5}$ and NO_x, as well as BC and NO_x as mentioned above, suggesting that the particles at the site ~~in Nanjing University Gulou Campus were~~are mainly associated with combustion sources (Wang et al., 2006; Ding et al., 2013b; Zhuang et al., 2014b).~~, which is also the reason for the negative correlation between particles and O_3.~~ It is found that high O_3 levels are generally ~~associated~~ related ~~with~~ to air masses of high CO/NO_x or particles/NO_x ratio~~,~~. An increase in CO, as well as $PM_{2.5}$ and BC, always results in higher O_3 concentration for NO_x lower than 40 ppb, while NO_x reverses. ~~and when NO_x concentrations was lower than 40 ppb, an increase in CO or particular matter concentrations would cause a sharp increase in O_3 concentrations while NO_x reverses.~~ To be specific, when NO_x reduces for CO lower than 1500 ppb, O_3 has a sharp increase, and an increase in the CO level would lead to an in increase in the O_3 concentration, especially when NO_x is lower than 40 ppb. The concentration of O_3 is sensitive to the level of its precursors, and the O_3 formation regime often includes NO_x-sensitive O_3 formation regime and VOCs-sensitive O_3 formation regime. If O_3 formation is under VOC-sensitive regime, a reduction in the NO_x concentration will lead to an increase in the O_3 concentration, which is used to determine the O_3 photochemical production in the

region is VOC-limited or NOx-limited based on observation data (Geng et al., 2008; Ding et al., 2013b). In our study, we have no VOCs measurement, thus CO is chosen as the reference tracer, because mixing ratios of CO showed significant correlations with the measured levels of most anthropogenic VOCs, which has been verified in many previous studies (e.g., Baker et al., 2008; von Schneidemesser et al., 2010; Wang et al., 2014). In addition, as a significant precursor of O_3, CO also plays a similar role as VOCs. HO_2 produced from the oxidation reaction of CO with OH radicals could initiate photochemical reactions which result in the net formation of O_3 (Novelli et al., 1998; Atkinson et al., 2000; Gao et al., 2005). Thus, the CO–O_3–NO_x relationship may reflect the correlation of VOCs, NO_x and O_3 in this region to some degree. And we suggest that the region is VOC-sensitive. ~~As discussed in Atkinson et.al (2000), volatile organic compounds (VOCs) generally have good correlation with CO and play a role similar to CO in the photochemical ozone production. Particles also have good correlation with CO, so the particles–O_3–NO_x relationship may indicate a VOC-sensitive regime of O_3 formation in this region, as the CO–O_3–NO_x relationship.~~ Geng et al. (2008) reported a VOC-sensitive regime in Shanghai combining the measured and modeling results~~by using measured and modeling results~~, and Ding et al. (2013b) also reported a VOC-sensitive regime in rural ~~area in~~ Nanjing using the observation data. And the $PM_{2.5}$-O_3-NO_x and BC-O_3-NO_x relationship show the similar pattern, possibly because they are well-correlated with CO.

~~Correlations of $PM_{2.5}$–O_3 in daytime when UV radiation is relatively strong and nighttime when UV radiation is approximately 0 are shown in Fig.10. It is found that the correlation is better with a clearer tendency and O_3 are higher during daytime, suggesting strong photochemistry progresses~~

~~during daytime. Some data in the nighttime plots show relatively high O_3. Most occurred in September and February when O_3 concentrations were extremely high. It is also found that some show relatively high NO_x associated with relatively low $PM_{2.5}$. After a further backward trajectories analysis (Section 3.4), we found that these data are most likely corresponded to air masses coming from the nearby and northwest in November and December, which may contain high NO_x plumes and transport to Nanjing during nighttime.~~

3.4 Backward Trajectories Analysis

The cluster means of the backward ~~trajectories~~ trajectory at 100 m from Gulou, Nanjing, in 2016 fall (Fig.11) and winter (Fig. 13) suggest different air flows ~~that were~~ transported to Nanjing from long distances. In general, the aerosol kinds and optical properties are characterized differently with different air masses in the two seasons, which are further analyzed by their origins in SON and DJF (Figs.12 and 14). Figs. 12 and 14 show the main concentrations of particles and trace gases, the ratio of $PM_{2.5}$ to PM_{10}, as well as the values of the aerosol optical properties of different clusters during SON and DJF, respectively. Because PM_{10} var~~y~~ies similarly to $PM_{2.5}$, while NO_x varies similaryly to NO_y, we only show the variations of $PM_{2.5}$ and NO_y with cluster ~~with cluster here~~. Also, because σ_a, σ_{ts} and σ_{bs} ~~AAC, SC and Bsp~~ have good correlations with particle concentrations (Zhuang et al., 2014a) and g ~~Asp~~ is greatly affected by relative humidity (RH), we discuss the variation of α_{ts} and ω_0 ~~SAE and SSA~~ with cluster here.

~~Most of air masses came from the oceans in fall (40 %, cluster 4 in Fig. 11) and from the north and north-west of China in winter (49 %, clusters 1 and 4 in Fig. 13). Although air masses came from north in both fall (cluster 4) and winter (cluster 4), the trajectory cluster in fall came from the oceans~~

~~more than the one in winter. In winter, considerable air masses arriving at the site were also from places near Nanjing (35%, cluster 2 in Fig. 13). Therefore, the aerosol kinds and optical properties at the study site are characterized differently with different air masses in the two seasons, which are further analyzed by their origins in SON and DJF (Figs.12 and 14).~~

~~Figs. 12 and 14 show the main concentrations of particles and trace gases, the ratio of $PM_{2.5}$ to PM_{10}, as well as the values of the aerosol optical properties of different clusters during SON and DJF, respectively. Because PM_{10} vary similarly to $PM_{2.5}$, while NO_x varies similaryly to NO_y, we only show the variations of $PM_{2.5}$ and NO_y with cluster here. Also, because AAC, SC and Bsp have good correlations with particle concentrations (Zhuang et al., 2014) and Asp is greatly affected by relative humidity (RH), we discuss the variation of SAE and SSA with cluster here.~~

In SON, the dominant air masses are from the East China Sea ~~(~~passing through urban agglomeration regions (cluster 3), and less-developed regions (cluster 2) of the YRD, and from northern continent away from Nanjing ~~(cluster 4)~~ ~~(~~passing through oceans and urban agglomeration regions (cluster 4)~~)~~. It is found that although air masses in cluster 3, cluster 4 and cluster 2 all pass through the oceans and have the same level of ~~relative humidity (~~RH~~)~~, differences still exist among the clusters. The air masses have to cross the urban agglomeration (from Shanghai to Nanjing) of YRD ~~when they arrive in~~before arriving in Nanjing in cluster 3 but ~~past~~ pass less-developed regions (north Jiangsu Province) in cluster 4 and cluster 2. In YRD, emissions of the aerosols and trace gases are much stronger in urban agglomeration regions than those in other areas (Zhang et al., 2009; Zhuang et al., 2013). It is also noticeable that concentrations of aerosols in cluster 4 are mostly lower, which

may result from its avoidance from BTH regions, also a megacities and urban agglomeration. In addition, air masses from the west of cluster 1 contain the highest ~~concentrations~~ levels of ~~particulate matter~~PMs and precursors~~, CO and NO_y, . which~~ Air masses ~~may result from~~ ~~crossing~~ pass central China with high emissions of ~~CO~~ particles and precursors ~~according to MERRA data (https://gmao.gsfc.nasa.gov/reanalysis/MERRA). Particulate matter and NO_y mainly have the same sources as CO,~~ according to MERRA data (https://gmao.gsfc.nasa.gov/reanalysis/MERRA) and Zhuang et al. (2018)~~, and h~~Also, high concentrations of these aerosols are also reflected in a high AOD according to the MISR data (https://giovanni.gsfc.nasa.gov/giovanni). ~~Zhuang et al. (2015) also suggested that high emission occurred in central China.~~ As for the ratio of $PM_{2.5}$ to PM_{10}, the ratio represents the ~~amount~~number of particles deriving from secondary pollution progress compared to those from primary pollution progress to some extent. In SON, ratios of clusters 1~3 are relatively close (all over 60%) with a maximum of cluster 3,~~Clusters 1-3 had relatively similar ratios in SON, all over 60% except cluster 4, with the maximum of cluster 3,~~ which means particles ~~deriving~~generating from secondary pollution progress in the three clusters have a similar rate. O_3 concentrations among the ~~four~~4 cluster were different. Despite negative correlations of O_3 with ~~its~~ precursors and particles, the concentrations of O_3 in cluster 3 was higher than in cluster 4, possibly because radiation in cluster 3 is stronger~~as UV in cluster 3 was higher that in cluster 4~~. The size of the aerosols in cluster 1 were finest (α_{ts} ~~SAE~~ is the largest in Fig. 12g), because the other three clusters ~~all pasted through oceans before arriving Nanjing, ~~are more humid going through oceans~~with higher relative humidity (RH)~~, making it easier for particles' hygroscopic growth. ω_0 ~~SSA~~ is also the largest in cluster 1, which means aerosols in cluster 1 are more scattering.

~~(https://giovanni.gsfc.nasa.gov/giovanni). Zhuang et al. (2015) also suggested that high emission~~

~~occurred in central China. As for the ratio of $PM_{2.5}$ to PM_{10}, the ratio represents the amount of particles deriving from secondary pollution progress compared to those from primary pollution progress. Clusters 1-3 had relatively similar ratios in SON, all over 60% except cluster 4, with the maximum of cluster 3, which means particles deriving from secondary pollution progress in the three clusters have a similar rate. O_3 concentrations among the four cluster were different. Despite negative correlations of O_3 with its precursors and particles, the concentrations of O_3 in cluster 3 was higher than in cluster 4, as UV in cluster 3 was higher that in cluster 4. The size of the aerosols in cluster 1 were finest (SAE is the largest in Fig. 12g), because the other three clusters all pasted through oceans before arriving Nanjing, with higher relative humidity (RH), making it easier for particles' hygroscopic growth. SSA is also the largest in cluster 1, which means aerosols in cluster 1 are more scattering.~~

In DJF, the air masses come from the local region ~~were from the places near Nanjing~~ (cluster 2), north-west areas~~northern continent away from Nanjing~~ (cluster 1), and northern regions~~northern continent away~~ far from Nanjing ~~passing through oceans and urban agglomeration regions~~ (cluster 4). Air masses from cluster 1 and cluster 2 both account for over 30% of the total aerosol characteristics and are more polluted with relatively high levels of particles, CO, and NO_x. Air masses in cluster 1 come from Shandong Province while those in cluster 2 come from local areas. Particles and trace gases concentrations of cluster 2 are higher than those of cluster 1 to some extent, implying the severer air pollution problem in YRD region. ~~This is different from that in SON. Therefore, besides what has been discussed of cluster 3 and cluster 4 in SON, it is found that air masses from cluster 1 and cluster 2 both account for over 30% of the total characteristics of the~~

~~aerosol optical properties and are main sources of pollutants in DJF (particles, CO, and NO_x are higher in Fig.14). Air masses in cluster 1 came from Shandong Province while those in cluster 2 came from areas nearby. Particles and trace gases concentrations of cluster 2 are higher than those of cluster 1 to some extent, which may result from the severer pollution in southern YRD than in Shandong Province.~~ The concentrations of O_3, similar to that in SON, is affected by radiation besides precursors levels. Thus, O_3 concentration in cluster 2 is a little higher than that in cluster 1. ~~was affected by the UV (O_3 concentrations in cluster 2 is a little higher than that in cluster 1 in Fig.14)~~. The ratios of $PM_{2.5}$ to PM_{10} of cluster 1 and cluster 2 are approximately equal in DJF, over 70%. The size of aerosols in cluster 1 and 2 are coarser, however, probably due to the higher RH (over 65%).~~finer without passing through oceans, so SAE are larger (Fig.12g).~~ Aerosols in cluster 1 are scatter to some extent compared to those in cluster 2. The trajectories of cluster 3 and cluster 4 are analogous to those in SON, respectively, but more polluted, probably due to more emissions in DJF especially in north China and weaker flow from ocean in DJF.

3.5 Case Study

For further understanding of the causes for high pollutants episodes, especially high particulate and O_3 episodes, detailed analysis of a typical episode from 2016 December 3-6 is presented in this section. ~~we choose a typical episode from 2016 December 3-6 for a detailed analysis.~~

Fig.15 (a) and (b) show that high O_3 concentrations (over 80 ppb) occurred on December 4 with

905 broad O_3 peaks (over 60 ppb) in the following days, while the average O_3 during the cold seasons
906 was 37.7 ppb. Though there is a lack of particulate matter concentrations because of the instrument
907 breakdown, ~~we could see the~~ high concentrations of ~~particulate matter~~PMs might possibly occur
908 referring to ~~from~~ the relatively high σ_e ~~EC~~ value (over 500 Mm^{-1}) and BC concentrations (over 6
909 $\mu g/m^3$) on December 4th~~,~~. ~~and b~~Both PMs reach a maximum on December 5th ($PM_{2.5}$ over 200
910 $\mu g/m^3$ and PM_{10} over 300 $\mu g/m^3$), over 3 times of the average concentrations. Besides, NO_x, NO_y,
911 have reached high levels since December 4th (NO_x over 70 ppb and NO_y over 100 ppb). It is also
912 noticeable that ω_0 ~~SSA~~ has a relatively sharp decrease from December 4th, especially on December
913 5th when particle concentrations were extremely high, ~~representing~~ probably suggesting that the
914 ratio of PM_{10} became higher. Meanwhile, a relatively sharp increase occurred in α_{ts} ~~SAE~~, without
915 any obvious variation in α_a ~~AAE~~, though, ~~which shows~~implying that scattering aerosols could take
916 the leading role during this episode.~~are the main components.~~ It is also found that this case occurred
917 under calm conditions before the passage of a cold front, which was ~~at~~ in the front of a continental
918 high pressure system originating from Mongolia and sweeping over Nanjing (Fig.15 (c~~)),~~)). ~~and~~
919 And the decrease in temperature with high pressure system dominating eastern China ~~were~~ wes also
920 detected on December 6th. Backward ~~trajectories~~ trajectory analysis for the past 96 hours (Fig.15
921 (d)) ~~were~~ was conducted ~~for~~ from December 5th at ~~8 pm~~20:00 LT, ~~for~~ including the maximum
922 concentrations of O_3 on December 4th and ~~particulate matter~~PMs on December 5th~~,~~. ~~which~~ It is
923 suggested that predominant wind was just in time from the NW directions. Therefore, air masses
924 with high particles and O_3 concentrations would be transported to Nanjing~~,~~. ~~which were~~It was also
925 clearly detected in Nanjing during these days, such as the relatively high O_3 during nighttime on
926 December 5th and 6th. The highest O_3 concentration on December 4th together with high particles

and primary pollutants NO_x and NO_y suggests a strong in situ photochemical production in mixed regional plumes under the influence of ~~high~~ the high-pressure system. Previous studies (Luo et al., 2000; Wang et al., 2006; Ding et al., 2013b) ~~Guo et al. (2009)~~ reported that the anticyclonic conditions, e.g., sunny weather and low wind velocities, are favorable for pollution accumulation and O_3 production. Results in this case clearly demonstrate sub-regional transport of primary and secondary air pollutants within the YRD region under such weather system.

4. Conclusion

In this study, particles (BC and PMs) and trace gases (O_3 and related precursors) in polluted seasons, are investigated based on continuous measurements of concentrations and optical properties in the urban area of Nanjing. The characteristics and underlying reasons are comprehensively discussed from perspectives of temporal variations, inter-species correlations, trajectories analysis, and case studies associated with weather data and Lagrangian dispersion modeling.

~~In this paper, an overview of particles and O_3 concentrations, together with trace gases, during 2016 the cold seasons in urban Nanjing, China, has been presented based on continuous measurements of aerosols concentrations and optical properties at the Gulou site. The particles, O_3 and trace gases concentrations are comprehensively characterized from perspectives of temporal variations, inter-species correlations, trajectories analysis, and case studies based on weather data and Lagrangian dispersion modeling.~~

Measurements show that average concentrations of PM_{10} was 86.3 μg/m^3, with BC and $PM_{2.5}$

accounting for 3% and 67%, respectively. 48 and 14 days of $PM_{2.5}$ and PM_{10} exceeded NAAQS-CN, respectively. The results suggested that both BC and PMs levels in Nanjing have decreased because of energy conservation since 2014. The average concentration of O_3 was 37.7 ppb with 40 days of exceedance. Precursor concentrations, including CO, NO_x and NO_y, averaged 753, 28.4, and 28.6 ppb, respectively. Contrast to particles, O_3 concentration has increased in urban Nanjing, implying a severer pollution in rural area and entire YRD region. All the aerosols have substantially monthly and diurnal variations. Both particles and precursors reached maximum values in December and minimum values in October due to higher emission and less precipitation. O_3 showed a peak in September because of stronger radiation. Diurnal variations of BC and PMs were similar with peaks around 7:00~9:00 and 22:00~0:00 LT. Both of the peaks were influenced by traffic emissions in rush hours and accumulation of air pollution especially at night-time. The peaks of PMs often occurred 1~ 2 h later than those of BC, possibly due to the production of secondary particles. Precursors and particles varied similarly in time, and the diurnal variation of O_3 was analogous to that of radiation with peak around 15:00 LT.

~~Measurements show that hourly mean particle concentrations, including BC, $PM_{2.5}$, and PM_{10} at Gulou site, Nanjing, China, are 2.602±1.720 μg/m³, 58.2±36.8 μg/m³, and 86.3±50.8 μg/m³, respectively, with ranges of 0.064-15.608 μg/m³, 0.8-256.2 μg/m³, and 1.1-343.4 μg/m³, respectively. During the six months, 48 and 14 days when $PM_{2.5}$ and PM_{10}, respectively, exceeded Class II NAAQS. Measurements also showed that hourly mean O_3 concentrations in urban Nanjing ranged from 0.2 to 235.7 ppb, with average concentrations of 37.7±33.5 ppb. There were 40 days excess of O_3 during the period, suggesting a severe air pollution problem in the region.~~

$PM_{2.5}$ has a quasi-power-law distribution with Vis under RH of different ranges. The correlation is stronger than that in a rural region in YRD, implying greater effects of air pollution on visibility in urban Nanjing. O_3 shows an anti-correlation with NO_x generally, but it tends to be positive with a relatively high temperature and low level of NO_x. $PM_{2.5}$ and BC are overall negatively correlated with O_3. A positive correlation between $PM_{2.5}$ and O_3 exists under high temperatures, while it is not found in BC-O_3 correlation. The negative correlation is related to the titration effect of high NO concentration, which is highly correlated with particles due to similar emission sources. And the negative correlation between $PM_{2.5}$ and UV suggests particles could decrease actinic flux of radiation, and thus inhibit the photolysis reactions near surface to degrees. The positive correlation implies the formation of secondary aerosols under the effects of the high concentrations of oxidants and solar radiation. BC is hard to be generated through chemical reactions, which might explain why the correlation between BC and O_3 is obscurer when temperature rises. An increase in CO, as well as $PM_{2.5}$ and BC, always results in higher O_3 concentration, while NO_x reverses, which indicates a VOC-sensitive regime for photochemical production of O_3 in urban Nanjing.

~~The correlation analysis shows a negative $PM_{2.5}$–Vis correlation as well as RH, both of which would promote the extinction coefficient. Negative O_3–NO_y correlation occurs when temperature is relatively low but the correlation becomes weaker when temperature becomes higher. $PM_{2.5}$–O_3–T correlations reveal the formation of secondary aerosols, especially fine particulate matter under high O_3 concentration and temperature conditions, while BC–O_3–T correlations not. CO–NO_y–O_3 and $PM_{2.5}$–NO_y–O_3 correlations suggest that a VOC-sensitive regime for photochemical production of O_3 in urban Nanjing.~~

Backward trajectories indicate that Nanjing could be affected by local air flow (35% in DJF) and long-distance air flows mostly from western (11% in SON), northwestern (31% in DJF), northern (up to 50 % in SON and DJF), eastern (40% in SON and 17% in DJF). Considerable air pollution in the urban area of Nanjing is due to local and sub-regional emissions. Basically, air masses from the oceans and remote or less-developed areas are relatively clean with low aerosols concentrations. α_{ts} at the site is usually low when the relative humidity of air masses is high, possibly suggesting the increased hygroscopicity and more secondary aerosols production under higher RH.

~~The backward trajectory analysis suggests that the prevailing winds in Nanjing were from the north and east during the cold seasons in 2016. Air masses that are either from the east without passing through the urban agglomeration and from northern without crossing BTH regions were clean with low pollution concentrations. In contrast, air masses from local regions were polluted in winter, suggesting a severe air quality problem in YRD region. SAE and SSA were further studied, indicating that particles from oceans were coarser and less scattering because the airmasses were under high RH condition and less secondary pollutants were produced.~~

A case study for a typical high O_3 and $PM_{2.5}$ episode in December 2016 illustrates the important influences of sub-regional transport of pollutants from strong source regions and local synoptic weather on the episode. Stable conditions such as an anticyclonic system make it easy for pollutants to accumulate in this region. Results from this case reveal the mechanisms of sub-regional transport of primary and secondary air pollutants within the YRD region.

Overall, this work highlights the interactions and mechanisms of various aerosols and metrological fields besides the important environmental impact from human activities and meteorological conditions in the urban area in YRD region. Considering both results in this study and previous work, it is suggested that collaborative control measures among different administrative regions are urgently needed including but not limited to energy conservation and reduction of pollution emissions to improve air quality in the western part of YRD region.

Data availability. The automobile numbers and GDP are from http://www.njtj.gov.cn/. Satellite CO data are available at: https://gmao.gsfc.nasa.gov/reanalysis/MERRA. The aerosols AOD data are available at: https://giovanni.gsfc.nasa.gov/giovanni. The Lagrangian dispersion model Hybrid Single-Particle Lagrangian Integrated Trajectory (HYSPLIT) was supplied by NOAA: http://ready.arl.noaa.gov/HYSPLIT_traj.php. The meteorological data for HYSPLIT are accessible from ftp://arlftp.arlhq.noaa.gov/pub/archives/gdas1.

Acknowledgements: This work was supported by the National Key R&D Program of China (2017YFC0209803, 2014CB441203, 2016YFC0203303), the National Natural Science Foundation of China (41675143, 91544230, 41621005). The authors would like to thank all members in the AERC of Nanjing University for maintaining instruments.

References:

Allen, R. J., Sherwood, S. C., Norris, J. R., and Zender, C.S.: Recent Northern Hemisphere tropical expansion primarily driven by black carbon and tropospheric ozone, Nature, 485,

doi:10.1038/nature11097, 350–353, 2012.

Anderson, T. L. and Ogren, J. A.: Determining aerosol radiative properties using the TSI 3563 integrating nephelometer, Aerosol Sci. Tech., 29, 57–69, 1998.

An, J., Zou, J., Wang, J., Lin, X., Zhu, B., 2015. Differences in ozone photochemical characteristics between the megacity Nanjing and its suburban surroundings, Yangtze River Delta, China. Environ. Sci. Pollut. Res. 22, 19607–19617.

~~Andrews, E., Sheridan, P. J., Fiebig, M., McComiskey, M., Ogren, J. A., Arnott, P., Covert, D., Elleman, R., Gasparini, R., Collins, D., Jonsson, H., Schmid, B., and Wang, J.: Comparison of methods for deriving aerosol asymmetry parameter, J. Geophys. Res., 111, D05S04, doi:10.1029/2004JD005734, 2006.~~

Arnott, W. P., Hamasha, K., Moosmuller, H., Sheridan, P. J., and Ogren, J. A.: Towards aerosol light-absorption measurements with a 7-wavelength aethalometer: evaluation with a photoacoustic instrument and 3-wavelength nephelometer, Aerosol Sci. Technol., 39, 17–29, doi:10.1080/027868290901972, 2005.

Atkinson, R.: Atmospheric chemistry of VOCs and NOx, Atmos.Environ., 34, 2063–2101, doi:10.1016/S1352-2310(99)00460-4, 2000.

Badarinath, K. V. S., Kharol, S. K., Chand, T. R. K., Parvathi, Y. G., Anasuya, T., and Jyothsna, A. N.: Variations in black carbon aerosol, carbon monoxide and ozone over an urban area of Hyderabad, India, during the forest fire season, Atmos. Res., 85(1), 18–26, 2007.

Baker, A. K., Beyersdorf, A. J., Doezema, L. A., Katzenstein, A., Meinardi, S., Simpson, I. J., Blake, D. R., Rowland, F. S.: Measurements of nonmethane hydrocarbons in 28 United States cities, Atmos. Environ., 2008, 42(1): 170–182.

~~Bond, T. C., Doherty, S. J., Fahey, D. W., Forster, P. M., Berntsen, T., DeAngelo, B. J., Flanner, M.~~

~~G., Ghan, S., Karcher, B., Koch, D., Kinne, S., Kondo, Y., Quinn, P. K., Sarofim, M. C., Schultz, M. G., Schulz, M., Venkataraman, C., Zhang, H., Zhang, S., Bellouin, N., Guttikunda, S. K., Hopke, P. K., Jacobson, M. Z., Kaiser, J. W., Klimont, Z., Lohmann, U., Schwarz, J. P., Shindell, D., Storlvmo, T., Warren, S. G., and Zender, C. S.: Bounding the role of black carbon in the climate system: A scientific assessment, J. Geophys. Res.: Atmos., 118, 5380–5552, doi:10.1002/jgrd.50171, 2013.~~

~~Bond, T. C., Streets, D. G., Yarber, K. F., Nelson, S. M.,Woo, J. H., and Klimont, Z.: A technology-based global inventory of black and organic carbon emissions from combustion, J. Geophys. Res., 109(D14), D14203, doi:10.1029/2003jd003697, 2004.~~

~~Castro, T., Madronich, S., Rivale, S., Muhlia, A., and Mar, B.: The influence of aerosols on photochemical smog in Mexico City, Atmos. Environ., 35, 1765–1772, 2001.~~

~~Chameides, W.L., Bergin, M., 2002. Soot takes center stage. Science 297 (5590), 2214-2215.~~

Chameides, W. L., Li, X., Tang, X., Zhou, X., Luo, C., Kiang, C. S., John, J. St., Saylor, R. D., Liu, S. C., Lam, K. S., Wang, T., and Giorgi, F.: Is ozone pollution affecting crop yields in China, Geophys. Res. Lett., 26, 867–870, 1999b.

Chameides, W. L., Yu, H., Liu, S. C., Bergin, M., Zhou, X., Mearns, L., Wang., G., Kiang, C. S., Saylor, R. D., Luo, C., Huang, Y., Steiner, A., and Giorgi, F.: Case study of the effects of atmospheric aerosols and regional haze on agriculture: An opportunity to enhance crop yields in China through emission controls?, PNAS, 96, 13626–13633, 1999a.

Chen, T.; He, J.; Lu, X.W.; She, J.F.; Guan, Z.Q. Spatial and Temporal Variations of PM2.5 and Its Relation to Meteorological Factors in the Urban Area of Nanjing, China. Int. J. Environ. Res. Public Health 2016, 13, 921.

Cheung, V.T.F., Wang, T., 2001. Observational study of ozone pollution at a rural site in the Yangtze Delta of China. Atmos. Environ. 35, 4947–4958.

Chow, J. C., Watson, J. G., Lowenthal, D. H., Chen, L.-W. A., Motallebi, N.: PM2.5 source profiles for black and organic carbon emission inventories. Atmospheric Environment, 2011, 45(31): 5407-5414.

Collaud Coen, M., Weingartner, E., Apituley, A., Ceburnis, D., Fierz-Schmidhauser, R., Flentje, H., Henzing, J. S., Jennings, S. G., Moerman, M., Petzold, A., Schmid, O., and Baltensperger, U.: Minimizing light absorption measurement artifacts of the Aethalometer: evaluation of five correction algorithms, Atmos. Meas. Tech., 3, 457–474, doi:10.5194/amt-3-457-2010, 2010.

Deng, J.J., Wang, T.J., Liu, L., Jiang, F.: Modeling heterogeneous chemical processes on aerosol surface. Particuology 8 (4), 308-318, 2010.

Deng, J., Wang, T., Jiang, Z., Xie, M., Zhang, R., Huang, X., Zhu, J., 2011. Characterization of visibility and its affecting factors over Nanjing, China. Atmospheric Research 101, 681-691.

~~Chan, C.K., Yao, X., 2008. Air pollution in mega cities in China. Atmos. Environ. 42, 1–42.~~

~~Collaud Coen, M., Weingartner, E., Apituley, A., Ceburnis, D., Fierz-Schmidhauser, R., Flentje, H., Henzing, J. S., Jennings, S. G., Moerman, M., Petzold, A., Schmid, O., and Baltensperger, U.: Minimizing light absorption measurement artifacts of the Aethalometer: evaluation of five correction algorithms, Atmos. Meas. Tech., 3, 457–474, doi:10.5194/amt-3-457-2010, 2010.~~

~~Crutzen P. 1973. A discussion of the chemistry of some minor constituents in the stratosphere and troposphere[J]. Pure Appl. Geophys., 106-108 (1): 1385-1399, doi: 10.1007/BF00881092.~~

~~Deng, J.J., Wang, T.J., Liu, L., Jiang, F.: Modeling heterogeneous chemical processes on aerosol surface. Particuology 8 (4), 308-318, 2010.~~

Derwent, R. G., Ryall, D. B., Jennings, S. G., Spain, T. G., and Simmonds, P. G.: Black carbon aerosol and carbon monoxide in European regionally polluted air masses at Mace Head,

Ireland during 1995–1998, Atmos. Environ., 35(36), 6371–6378, 2001.

Ding, A. J., Fu, C. B., Yang, X. Q., Sun, J. N., Zheng, L. F., Xie, Y. N., Herrmann, E., Nie, W., Petaja, T., Kerminen, V. -M., and Kulmala, M.: Ozone and fine particle in the western Yangtze River Delta: an overview of 1 yr data at the SORPEs station, Atmos. Chem. Phys., 13, 5813–5830, 2013b.

Draxler, R. R. and Hess, G. D.: An overview of the HYSPLIT 4 modeling system for trajectories dispersion and deposition, Aust. Meteoro. Mag., 47, 295–308, 1998.

Draxler, R.R. and Rolph, G.D. (2013) HYSPLIT (HYbrid Single-Particle Lagrangian Integrated Trajectory) Model Access Via NOAA ARL READY Website, NOAA Air Resources Laboratory, Silver Spring, MD [online].

Eichler, H., Cheng, Y. F., Birmili,W., Nowak, A.,Wiedensohler, A., Brüggemann, E., Gnauk, T., Herrmann, H., Althausen, D., Ansmann, A., Engelmann, R., Tesche, M., Wendisch, M., Zhang, Y. H., Hu, M., Liu, S., and Zeng, L. M.: Hygroscopic properties and extinction of aerosol particles at ambient relative humidity in South-Eastern China, Atmos. Environ., 42, 25, 6321–6334. doi:10.1016/j.atmosenv.2008.05.007, 2008.

Gao, J., Wang, T., Ding, A., and Liu, C.: Observational study of ozone and carbon monoxide at the summit of mount Tai (1534 m a.s.l.) in central-eastern China. Atmos. Environ.39, 4779–4791, 2005.

Geng, F.H., Tie, X.X., Xu, J.M., Zhou, G.Q., Peng, L., Gao, W., Tang, X., Zhao, C.S.: Characterizations of ozone, NOx, and VOCs measured in Shanghai, China. Atmos. Environ. 42, 6873–6883, 2008.

Gong, W., Zhang, T.H., Zhu, Z.M., Ma, Y.Y, Ma, X., Wang, W.: Characteristics of PM1.0, PM2.5

and PM10 and their relation to black carbon in Wuhan, central China. Atmosphere, 2015, 6(9): 1377-1387.

Guo, H., Wang, T., Simpson, I., Blake, D., Yu, X., Kwok, Y., et al., 2004b. Source contributions to ambient VOCs and CO at a rural site in eastern China. Atmos. Environ. 38, 4551–4560.

Han, S., 2011. Analysis of the relationship between O3, NOandNO2 in Tianjin, China. Aerosol Air Qual. Res.

Huang, F., Li, X., Wang, C., Xu, Q., Wang, W., Luo, Y., Tao, L., Gao, Q., Guo, J., Chen, S.: PM2.5 spatiotemporal variations and the relationship with meteorological factors during 2013–2014 in Beijing, China. PLoS ONE 2015, 10, e0141642.

Huang, X., Li, M., Li, J., Song, Y.: A high-resolution emission inventory of crop burning in fields in China based on MODIS Thermal Anomalies/Fire products. Atmospheric Environment, 2012, 50:9-15.

Huang, X. X., Wang, T. J., Jiang, F., Liao, J. B., Cai, Y. F., Yin, C. Q., Zhu, J. L., Han, Y., 2013. Studies on a severe dust storm in East Asia and its impact on the air quality of Nanjing, China. Aerosol Air Qual. Res. 13, 179e193.

~~Jacobson, M.Z., 2002. Control of fossil-fuel particulate black carbon and organic matter, possibly the most effective method of slowing global warming. Journal of Geophysical Research 107 (D19), 4410.~~

~~Jacobson, M. Z.: Studying the effects of aerosols on vertical photolysis rate coefficient and temperature profiles over an urban airshed, J. Geophys. Res., 103, 10593–10604, doi:10.1029/9 5 8JD00287, 1998.~~

Jennings, S. G., Spain, T. G., Doddridge, B. G., Maring, H., Kelly,B. P., and Hansen, A. D. A.: Concurrent measurements of black carbon aerosol and carbon monoxide at Mace Head, J. Geophys. Res.-Atmos., 101(D14), 19447–19454, 1996.

Jennings, S. G., Spain, T. G., Doddridge, B. G., Maring, H., Kelly,B. P., and Hansen, A. D. A.: Concurrent measurements of black carbon aerosol and carbon monoxide at Mace Head, J.

Geophys. Res. Atmos., 101(D14), 19447–19454, 1996.

Jerrett, M., Finkelstein, M. M., Brook, J. R., Arain, M. A., Kanaroglou, P., Stieb, D. M., Gilbert, N. L., Verma, D., Finkelstein, N., Chapman, K. R., and Sears, M. R.: A Cohort Study of Traffic-Related Air Pollution and Mortality in Toronto, Ontario, Canada. Environmental Health Perspectives, 2009, 117(5):772-777.

Jiang, J., Zheng, Y.F., Liu, J.J., and Fan, J.J.: Observational research on planetary boundary layer by lidar over Nanjing city. Environ. Sci. Technol. 37, 22–27 (in Chinese), 2014.

Jiang, L., Zhang, Z. F., Zhu, B., Shen, Y., Wang, H. L., Shi, S. S., Sha, D. D.: Comparison of parameterizations for the atmospheric extinction coefficient in Lin'an, China. The Science of the total environment., 2018, 621. 507-515. 10.1016/j.scitotenv.2017.11.182.

Kaufman, Y.J.; Tanré, D.; Boucher, O. A satellite view of aerosols in the climate system. Nature 2002, 419, 215–223.

~~Kristjánsson, J.E., 2002. Studies of the aerosol indirect effect from sulfate and black carbon aerosols. Journal of Geophysical Research 107 (D15), 4246.~~

Khoder, M. I.: Atmospheric conversion of sulfur dioxide to particulate sulfate and nitrogen dioxide to particulate nitrate and gaseous nitric acid in an urban area, Chemosphere, 49, 675–684, 2002.

Kristjánsson, J.E., 2002. Studies of the aerosol indirect effect from sulfate and black carbon aerosols. Journal of Geophysical Research 107 (D15), 4246.

Kumar, R., Barth, M.C., Madronich, S., Naja, M., Carmichael, G.R., Pfister, G.G., Knote, C., Brasseur, G.P., Ojha, N., Sarangi, T., 2014. Effects of dust aerosols on tropospheric chemistry during a typical pre-monsoon season dust storm in northern India. Atmos. Chem. Phys. 14, 6813-6834.

~~Lal, S., Naja, M., and Subbaraya, B.H.: Seasonal variations in surface ozone and its precursors over~~

~~an urban site in India. Atmos. Environ. 34, 2713–2724, 2000.~~

~~Lam, K.S., Wang, T.J., Chan, L.Y., Wang, T., and Harris, J.: Flow patterns influencing the seasonal behavior of surface ozone and carbon monoxide at a coastal site near Hong Kong. Atmos. Environ. 35, 3121–3135, 2001.~~

Larson, S.M., and Cass, G.R.: Characteristics of summer midday low-visibility events in the Los Angeles area. Environmental Science & Technology. 23-281, 1989.

Liao, H., Seinfeld, J.H., 2005. Global impacts of gas-phase chemistry aerosol interactions on direct radiative forcing by anthropogenic aerosols and ozone. Journal of Geophysical Research 110, D18208.

Li, G.H., Zhang, R.Y., and Fan, J.W.: Impacts of black carbon aerosol on photolysis and ozone. [J]. Journal of Geophysical Research. Vol. 110, D23206, doi:10.1029/2005JD005898, 2005.

Li, J., Bo, Y., Xie, S.: Estimating emissions from crop residue open burning in China based on statistics and MODIS fire products. Journal of Environmental Sciences, 2016, 44:158-167.

Li, J., Wang, Z., Wang, X., Yamaji, K., Takigawa, M., Kanaya, Y., Pochanart, P., Liu, Y., Irie, H., Hu, B., Tanimoto, H., and Akimoto, H.: Impacts of aerosols on summertime tropospheric photolysis frequencies and photochemistry over Central Eastern China, Atmos. Environ., 45, 1817–1829, doi:10.1016/j.atmosenv.2011.01.016, 2011.

Li, M., Wang, T., Xie, M., Li, S., Zhuang, B., Chen, P.: Agricultural fire impacts on ozone photochemistry over the Yangtze River Delta region, East China. Journal of Geophysical Research: Atmospheres, 2018.

Li, M., Wang, T., Xie, M., Li, S., Zhuang, B., Chen, P.: Impacts of aerosol-radiation feedback on local air quality during a severe haze episode in Nanjing megacity, eastern China, Tellus B: Chemical and Physical Meteorology, 2017, 69(1):1339548.

Li, M., Zhang, Q., Kurokawa, J., Woo, J.-H., He, K. B., Lu, Z. F., Ohara, T., Song, Y., Streets, D.

G., Carmichael, G. R., Cheng, Y. F., Hong, C. P., Huo, H., Jiang, X. J., Kang, S., Liu, F., Su, H., Zheng, B.: MIX: a mosaic Asian anthropogenic emission inventory under the international collaboration framework of the MICS-Asia and HTAP, Atmos. Chem. Phys., 2017, 17, 935–963.

~~Lin,W., Xu, X., Ge, B., Zhang, X., 2009. Characteristics of gaseous pollutants at Gucheng, a rural site southwest of Beijing. J. Geophys. Res. Atmos. 114, D00G14.~~

Lin, W., Xu, X., Zhang, X., Tang, J., 2008. Contributions of pollutants from North China Plain to surface ozone at the Shangdianzi GAW Station. Atmos. Chem. Phys. 8, 5889–5898.

Liu, P. F., Zhao, C. S., Gobel, T., Hallbauer, E., Nowak, A., Ran, L., Xu, W. Y., et al.: Hygroscopic properties of aerosol particles at high relative humidity and their diurnal variations in the North China Plain, Atmos. Chem. Phys., 3479–3494, doi:10.5194/acp-11-3479-2011, 2011.

Luo, C., St. John, J. C., Zhou, X. J., Lam, K. S., Wang, T., and Chameides, W. L.: A nonurban ozone air pollution episode over eastern China: Observation and model simulation, J. Geophys. Res., 105, 1889–1908, 2000.

~~Ma, J.Z., Xu, X.B., Zhao, C.S., Yan, P., 2012. A review of atmospheric chemistry research in China: photochemical smog, haze pollution, and gas-aerosol interactions. Adv. Atmos. Sci. 29, 1006–1026.~~

Mcgowan, H. and Clark, A.: Identification of dust transport pathways from Lake Eyre, Australia using Hysplit, Atmos. Environ., 42, 6915–6925, 2008.

Meng, Z.Y., Xu, X.B., Yan, P., Ding, G.A., Tang, J., Lin, W.L., et al., 2009. Characteristics of trace gaseous pollutants at a regional background station in Northern China. Atmos.Chem. Phys. 9, 927–936.

Ministry of Environmental Protection of China (MEP), Ambient air quality standards (GB 3095–2012), 12 pp., China Environmental Science Press, Beijing, 2012.

Müller, T., Laborde, M., Kassell, G., and Wiedensohler, A.: Design and performance of a three-wavelength LED-based total scatter and backscatter integrating nephelometer, Atmos. Meas.

Tech., 4, 1291–1303, doi:10.5194/amt-4-1291-2011, 2011.

~~Monks, P.S., Archibald, A.T., Colette, A., Cooper, O., Coyle, M., Derwent, R., Fowler, D., Granier, C., Law, K.S., Mills, G.E., Stevenson, D. S., Tarasova, O., Thouret, V., von Schneidemesser, E., Sommariva1, R., Wild, O., and Williams, M. L.: Tropospheric ozone and its precursors from the urban to the globalscale from air quality to short-lived climate forcer, Atmos. Chem. Phys., 15, 8889–8973, doi:10.5194/acp-15-8889-2015, 2015.~~

~~Tropospheric ozone and its precursors... (PDF Download Available). Available from: https://www.researchgate.net/publication/278623484_Tropospheric_ozone_and_its_precursors_from_the_urban_to_the_global_scale_from_air_quality_to_short-lived_climate_forcer#pf1 [accessed Jun 24 2018].~~

Novelli, P.C., Masari1ea, K. A., Lang, P.M.: Distributions and recent changes of carbon monoxide in the lower troposphere. Journal of Geophysical Research Atmospheres, 1998, 103(D15).

Pan, X.L., Kanaya, Y., Wang, Z.F., Liu, Y., Pochanart, P., Akimoto, H., Sun, Y.L., Dong, H.B., Li, J., Irie, H., Takigawa, M., 2011. Correlation of black carbon aerosol and carbon monoxide in the high-altitude environment of Mt. Huang in Eastern China. Atmospheric Chemistry and Physics 11, 9735-9747.

Petzold, A., Kopp, C., and Niessner, R.: The dependence of the specific attenuation cross-section on black carbon mass fraction and particle size, Atmos. Environ., 31, 661–672, 1997.

Qian, L., Yan, Y., and Qian, J.M.: An Observational Study on Physical and Optical Properties of Atmospheric Aerosol in Autumn in Nanjing [J]. Meteorological and Environmental Research 2014, 5(2): 24 − 30.

Roberts, P. T., Friedlander, S. K.: Analysis of sulfur in deposited aerosol particles by vaporization and flame photometric detection. Atmospheric Environment, 1976, 10(5), 403-408.

Sassen, K., 2002. Indirect climate forcing over the western US from Asian dust storms. Geophys.. Res. Lett. 29.

Schleicher, N., Cen, K., Norra, S.: Daily variations of black carbon and element concentrations of atmospheric particles in the Beijing megacity – Part 1: General temporal course and source identification. Chemie der Erde - Geochemistry, 2013, 73(1):51-60.

Schmid, O., Artaxo, P., Arnott,W. P., Chand, D., Gatti, L. V., Frank, G. P., Hoffer, A., Schnaiter, M., and Andreae, M. O.: Spectral light absorption by ambient aerosols influenced by biomass burning in the Amazon Basin. I: Comparison and field calibration of absorption measurement techniques, Atmos. Chem. Phys., 6, 3443–3462, doi:10.5194/acp-6-3443-2006, 2006.

Shao, M., Tang, X., Zhang, Y., Li, W., 2006. City clusters in China: air and surface water pollution. Front. Ecol. Environ. 4, 353–361.

Shen, G. F., Yuan, S. Y., Xie, Y. N., Xia, S. J., Li, L., Yao, Y. K., Qiao, Y. Z., Zhang, J., Zhao, Q.Y., Ding, A. J.: Ambient levels and temporal variations of PM2.5 and PM10 at a residential site in the mega-city, Nanjing, in the western Yangtze River Delta, China. J. Environ. Sci. Health Part A 2014, 49, 171–178.

Shi, C., Wang, S., Liu, R., Zhou, R., Li, D., Wang, W., et al., 2015. A study of aerosol optical properties during ozone pollution episodes in 2013 over Shanghai, China. Atmos. Res. 153, 235–249.

~~Schneidemesser, E., Sommariva, R., Wild, O., and Williams, M. L.: Tropospheric ozone and its precursors from the urban to the global scale from air quality to short-lived climate forcer, Atmos. Chem. Phys., 15, 8889–8973, doi:10.5194/acp-15-8889-2015, 2015.~~

Song, W.; Jia, H.; Huang, J.; Zhang, Y. A satellite-based geographically weighted regression model for regional PM2.5 estimation over the Pearl River Delta region in China. Remote Sens. Environ. 2014, 154, 1–7.

Spackman, J. R., Schwarz, J. P., Gao, R. S., Watts, L. A., Thomson, D. S., Fahey, D. W., Holloway,

J. S., de Gouw, J. A., Trainer, M., and Ryerson, T. B.: Empirical correlations between black carbon aerosol and carbon monoxide in the lower and middle troposphere, Geophys. Res. Lett., 35(19), L19816, doi:10.1029/2008GL035237, 2008.

Stein, A. F., Draxler, R. R., Rolph, G. D., Stunder, B. J. B., Cohen, M. D., and Ngan, F.: NOAA'S Hysplit Atmospheric Transport and Dispersion Modeling System, Bull. Amer. Meteor. Soc., 96, 2059–2077. doi: http://dx.doi.org/10.1175/BAMS-D-14-00110.1, 2016.

Streets, D.G., Gupta, S., Waldhoff, S.T., Wang, M.Q., Bond, T.C., Bo, Y.Y., 2001. Black carbon emissions in China. Atmospheric Environment 35, 4281-4296.

Tegen, I., Schepanski, K.:The global distribution of mineral dust. IOP Conference Series: Earth and Environmental Science, 2009, 7:012001.

Tu, J., Xia, Z. G., Wang, H. S., and Li, W. Q.: Temporal variations in surface ozone and its precursors and meteorological effects at an urban site in China, Atmos. Res., 85, 310–337, 2007.

van Donkelaar, A., Martin, R. V., Brauer, M., Kahn, R., Levy, R., Verduzco, C., and Villeneuve, P. J.: Global estimates of ambient fine particulate matter concentrations from satellite-based aerosol optical depth: development and application, Environ. Health Perspectives, 118, 847–855, 2010.

Verma, R.L., Sahu, L.K., Kondo, Y., Takegawa, N., Han, S., Jung, J.S., Kin, Y.J., Fan, S., Sugimoto, N., Shammaa, M.H., Zhang, Y.H., Zhao, Y., 2010. Temporal variations of black carbon in Guangzhou, China, in summer 2006. Atmospheric Chemistry and Physics 10, 6471-6485.

~~Virkkula, A., Makela, T., Hillamo, R., Yli-Tuomi, T., Hirsikko, A., Hameri, K., and Koponen, I. K.: A simple procedure for correcting loading effects of aethalometer data, J. Air Waste Manage., 57, 1214–1222, doi:10.3155/1047-3289.57.10.1214, 2007.~~

von Schneidemesser, E., Monks, P. S., and Plass-Duelmer, C.: Global comparison of VOC and CO

observations in urban areas, Atmos. Environ., 2010, 44(39): 5053–5064.

Wang, G. H., Huang, L. M., Gao, S. X., Gao, S. T., and Wang, L.S.: Characterization of watersoluble species of PM10 and PM2.5aerosols in urban area in Nanjing, China, Atmos. Environ., 36,1299–1307, 2002.

Wang, H. L., Zhuang, Y. H., Wang, Y., Sun, Y. L., Yuan, H., Zhuang, G. S., Hao, Z. P.: Long-term monitoring and source apportionment of PM 2.5/PM 10 in Beijing, China. Journal of Environmental Sciences, 2008, 20(11): 1323-1327.

Wang, M., Shao, M., Chen, W., Yuan, B., Lu, S., Zhang, Q., Zeng, L., Wang, Q.: A temporally and spatially resolved validation of emission inventories by measurements of ambient volatile organic compounds in Beijing, China. Atmos. Chem. Phys., 2014, 14(12): 5871–5891.

Wang, M.Y., Cao, C.X., Li, G.S., and Singh, R.P.: Analysis of a severe prolonged regional haze episode in the Yangtze River Delta, China, Atmos. Environ., 102, 112-121, 2015.

Wang, P., Zhao, W.: Assessment of ambient volatile organic compounds (VOCs) near major roads in urban Nanjing, China[J]. Atmospheric Research, 2008, 89(3):0-297.

Wang, T., Cheung, V.T.F., Anson, M., Li, Y.S., 2001a. Ozone and related gaseous pollutants in the boundary layer of eastern China: overview of the recent measurements at a rural site. Geophys. Res. Lett. 28, 2373–2376.

Wang, T., Cheung, T., Li, Y., Yu, X., Blake, D., 2002. Emission characteristics of CO, NOx, SO2 and indications of biomass burning observed at a rural site in eastern China. J. Geophys. Res.-Atmos. 107.

Wang, T., Poon, C.N., Kwok, Y.H., Li, Y.S., 2003. Characterizing the temporal variability and emission patterns of pollution plumes in the Pearl River Delta of China. Atmos. Environ.37, 3539–3550.

Wang, T., Wong, C., Cheung, T., Blake, D., Arimoto, R., Baumann, K., et al., 2004. Relationships of trace gases and aerosols and the emission characteristics at Lin'an, a rural site in eastern China, during spring 2001. J. Geophys. Res.-Atmos. 109.

Wang, T., Xue, L. K., Brimblecombe, P., Lam, Y.F., Li, L., and Zhang, L.: Ozone pollution in China: A review of concentrations, meteorological influences, chemical precursors, and effects. Science of the Total Environment., 575, 1582–1596, 2017.

~~Wang, T.J., Lam, K.S., Xie, M., Wang, X.M., Carmichael, G., and Li, Y.S.: Integrated studies of a photochemical smog episode in Hong Kong and regional transport in the Pearl River Delta of China. Tellus Ser. B Chem. Phys. Meteorol. 58, 31–40, 2006.~~

Wang, T. J., Zhuang, B. L., Li, S., Liu, J., Xie, M., Yin, C. Q., Zhang, Y., Yuan, C., Zhu, J. L., Ji, L. Q., and Han, Y.: The interactions between anthropogenic aerosols and the East Asian summer monsoon using RegCCMS. J. Geophys. Res. Atmos., 120, doi:10.1002/2014JD022877, 2015.

Wang, X., Li, J., Zhang, Y., Xie, S., Tang, X., 2009b. Ozone source attribution during a severe photochemical smog episode in Beijing, China. Sci. China, Ser. B: Chem. 52, 1270–1280.

Wang, Y.Q., Stein, A.F., Draxler, R.R., de la Rosa, J.D., amd Zhang, X.Y.: Global sand and dust storms in 2008: Observation and HYSPLIT model verification, Atmos. Environ., 45, 6368-6381, 2011.

Wang, Y., Ying, Q., Hu, J., Zhang, H.: Spatial and temporal variations of six criteria air pollutants in 31 provincial capital cities in China during 2013–2014. Environment International, 2014, 73:413–422.

Wang, Y., Wang, X., Kondo, Y., Kajino, M., Munger, J.W., Hao, J., 2011b. Black carbon and its correlation with trace gases at a rural site in Beijing: top-down constraints from ambient measurements on bottom-up emissions. Journal of Geophysical Research 116, D24304.

Wang, Y., Zhuang, G. S., Zhang, X. Y., Huang, K., Xu, Chang, Tang, A. H., Chen, J. M., and An, Z. S.: The ion chemistry, seasonal cycle, and sources of PM2.5 and TSP aerosol in Shanghai, Atmos. Environ., 40, 2935–2952, 2006.

Wang, Z., Li, J., Wang, X., Pochanart, P., Akimoto, H.: Modeling of Regional High Ozone Episode Observed at Two Mountain Sites (Mt. Tai and Huang) in East China. Journal of Atmospheric Chemistry, 2006, 55(3):253-272.

Wang, Z., Li, Y., Chen, T., Zhang, D., Sun, F., Pan, L.: Spatial-temporal characteristics of PM2.5 in Beijing in 2013. Acta Geogr. Sin. 2015, 70, 110–120.

Weingartner, E., Saathoff, H., Schnaiter, M., Streit, N., Bitnar, B., and Baltensperger, U.: Absorption of light by soot particles: determination of the absorption coefficient by means of aethalometers, J. Aerosol Sci., 34, 1445–1463, doi:10.1016/S0021- 8502(03)00359-8, 2003.

Wu, D., Liu, Q., Lian, Y., Bi, X., Li, F., Tan, H., Liao, B., Chen, H., Hazy weather formation and visibility deterioration resulted from fine particulate (PM2.5) pollutions in Guangdong and Hong Kong. J. Environ. Sci. Circumst. 2012, 32, 2660–2669.

~~Wu, D., Wu, C., Liao, B., Chen, H.,Wu, M., Li, F., Tan, H., Deng, T., Li, H., Jiang, D., and Yu, J. Z.: Black carbon over the South China Sea and in various continental locations in South China, Atmos. Chem. Phys., 13, 12257–12270, doi:10.5194/acp-13-12257-2013, 2013.~~

Wu, Y.; Guo, J.; Zhang, X.; Tian, X.; Zhang, J.; Wang, Y.; Duan, J.; Li, X. Synergy of satellite and ground based observations in estimation of particulate matter in eastern China. Sci. Total Environ. 2012, 433, 20–30.

Xiao, Z., Bi, X., Feng, Y., Wang, Y., Zhou, J., Fu, X., Weng, Y., 2012. Source apportionment of ambient PM10 and PM2.5 in urban area of Ningbo City. Res. Environ. Sci. (China) 5, 549–555.

Xiao, Z. M., Zhang, Y. F., Hong, S. M., Bi, X. H., Jiao, L., Feng, Y. C., Wang, Y. Q.: Estimation of the Main Factors Influencing Haze, Based on a Long-term Monitoring Campaign in Hangzhou, China. Aerosol & Air Quality Research., 2011, 11, 873-882.

Xie, M., Zhu, K.G., Wang, T.J., Chen, P.L., Han, Y., Li, S., Zhuang, B.L., and Shu, L., Temporal

characterization and regional contribution to O3 and NOx at an urban and a suburban site in Nanjing, China. Science of the Total Environment., 551–552, 533–545, 2016.

Xue, L., Wang, T., Louie, P.K.K., Luk, C.W.Y., Blake, D.R., Xu, Z., 2014a. Increasing external effects negate local efforts to control ozone air pollution: a case study of Hong Kong and implications for other Chinese cities. Environ. Sci. Technol. 48, 10769–10775.

Yang, S. J., He, H. P, Lu, S. L., Chen, D., Zhu, J. X.: Quantification of crop residue burning in the field and its influence on ambient air quality in Suqian, China. Atmospheric Environment, 2008,42(9):1961-1969.

Yan, S.; Cao, H.; Chen, Y.; Wu, C.; Hong, T.; Fan, H. Spatial and temporal characteristics of air quality and air pollutants in 2013 in Beijing. Environ. Sci. Pollut. Res. 2016, 23, 1–12.

Yin, S., Wang, X.F, Xiao, Y., Tani, H., Zhong, G.S., Sun, Z.Y.: Study on spatial distribution of crop residue burning and PM2.5 change in China. Environmental Pollution, 2016, 220(Pt A):204-221.

~~Yang, Y., Liu, X., Qu, Y., Wang, J., An, J., Zhang, Y., Zhang, F.: Formation mechanism of continuous extreme haze episodes in the megacity Beijing, China, in January 2013. Atmos. Res. 155, 192–203, 2015.~~

~~Yan, P., Tang, J., Huang, J., Mao, J. T., Zhou, X. J., Liu, Q., Wang, Z. F., and Zhou, H. G.: The measurement of aerosol optical properties at a rural site in Northern China, Atmos. Chem. Phys., 8, 2229–2242, doi:10.5194/acp-8-2229-2008, 2008.~~

Yi, R., Wang, Y. L., Zhang, Y. J., Shi, Y., Li, M. S., 2015. Pollution characteristics and influence factors of ozone in Yangtze River Delta. Acta Sci. Circumst. 35, 2370–2377 (in Chinese).

Yu, J., Wang, W., Zhou, J., Xu, D., Zhao, Q., He, L., 2015. Analysis of pollution characteristics and sources of PM2.5 in winter of Ningbo City. Environ. Sci. Technol. (China) 8, 150–155.

Zhang, Q., Streets, D.G., Carmichael, G.R., He, K.B., Huo, H., Kannari, A., Klimont, Z., Park, I.S., Reddy, S., Fu, J.S., Chen, D., Duan, L., Lei, Y., Wang, L.T., Yao, Z.L., 2009. Asian emissions in 2006 for the NASA INTEX-B mission. Atmos. Chem. Phys. 9, 5131–5153.

Zhang, Y. H., Hu, M., Zhong, L. J., Wiedensohler, A., Liu, S. C., Andreae, M. O., Wang, W., Fan, S. J.: Regional integrated experiments on air quality over Pearl River Delta 2004 (PRIDE-PRD2004): overview. Atmos. Environ. 42, 6157–6173, 2008.

Zhang, X. Y., Wang, Y. Q., Niu, T., Zhang, X. C., Gong, S.L., Zhang, Y.M., Sun, T.Y., 2012. Atmospheric aerosol compositions in China: spatial/temporal variability, chemical signature, regional haze distribution and comparisons with global aerosols. Atmospheric Chemistry and Physics 12, 779-799.

Zhang, X.Y., Wang, Y.Q., Zhang, X.C., Guo, W., Gong, S.L., 2008. Carbonaceous aerosol composition over various regions of China during 2006. Journal of Geophysical Research 113, D14111.

Zhang, Y. L., Cao, F. Fine particulate matter (PM2.5) in China at a city level. Sci. Rep. 2015, 5, 14884.

Zhang, Y., Shao, K., Tang, X., 1998. The study of urban photochemical smog pollution in China. Acta Scientiarum Naturalium-Universitatis Pekinensis 34, 392–400.

Zheng, J., Zhong, L., Wang, T., Louie, P.K.K., Li, Z., 2010. Ground-level ozone in the Pearl River Delta region: analysis of data from a recently established regional air quality monitoring network. Atmos. Environ. 44, 814–823.

~~Zhang, Y.H., Hu, M., Zhong, L.J., Wiedensohler, A., Liu, S.C., Andreae, M.O., Wang, W., Fan, S.J.: Regional integrated experiments on air quality over Pearl River Delta 2004 (PRIDE-PRD2004): overview. Atmos. Environ. 42, 6157–6173, 2008.~~

Zhu, J. L., Wang, T. J., Talbot, R. H., Mao, H. T., Hall, C. B., Yang, X. Q., Fu, C. B., Zhuang, B. L., Li, S., Han, Y., Huang, X., 2012. Characteristics of atmospheric Total Gaseous Mercury (TGM) observed in urban Nanjing, China. Atmospheric Chemistry and Physics 12, 12103-

12118.

Zhuang, B.L., Liu, L., Shen, F.H., Wang, T.J., Han, Y., 2010. Semidirect radiative forcing of internal mixed black carbon cloud droplet and its regional climatic effect over China. Journal of Geophysical Research 115, D00K19.

Zhuang, B.L., Liu, Q., Wang, T.J., Yin, C.Q., Li, S., Xie, M., Jiang, F., Mao, H.T., 2013. Investigation on semi-direct and indirect climate effects of fossil fuel black carbon aerosol over China. Theoretical and Applied Climatology 114, 651-672.

Zhuang, B. L., Li, S., Wang, T. J., Deng, J. J., Xie, M., Yin, C. Q., and Zhu, J. L.: Direct radiative forcing and climate effects of anthropogenic aerosols with different mixing states over China, Atmos. Environ., 79, 349–361, doi:10.1016/j.atmosenv.2013.07.004, 2013b.

Zhuang, B. L., Li, S., Wang, T. J, Liu, J., Chen, H. M., Chen, P. L., Li, M. M., Xie, M.: Interaction between the Black Carbon Aerosol Warming Effect and East Asian Monsoon Using RegCM4. Journal of Climate, 2018, 31(22):9367-9388.

Zhuang, B. L., Wang, T. J., Liu, J., Li, S., Xie, M., Han, Y., Chen, P. L., Hu, Q. D., Yang X.Q., Fu, C. B., and Zhu, J. L.: The surface aerosol optical properties in the urban area of Nanjing, west GTH River Delta, China. Atmos. Chem. Phys., 17, 1143–1160, doi:10.5194/acp-17-1143-2017, 2017.

Zhuang, B. L., Wang, T. J., Liu, J., Li, S., Xie, M., Yang, X. Q., Fu, C. B., Sun, J. N., Yin, C. Q., Liao, J. B., Zhu, J. L., and Zhang, Y.: Continuous measurement of black carbon aerosol in urban Nanjing of Yangtze River Delta, China, Atmos. Environ., 89, 415–424, 2014b.

Zhuang, B. L., Wang, T. J., Liu, J., Ma, Y., Yin, C. Q., Li, S., Xie, M., Han, Y., Zhu, J. L., Yang, X. Q., and Fu, C. B.: Absorption coefficient of urban aerosol in Nanjing, west Yangtze River Delta, China, Atmos. Chem. Phys., 15, 13633–13646, doi:10.5194/acp-15-13633-2015, 2015.

Zhuang, B. L., Wang, T. J., Li, S., Liu, J., Talbot, R., Mao, H. T., Yang, X. Q., Fu, C. B., Yin, C. Q.,

Zhu, J. L., Che, H. Z., and Zhang, X. Y.: Optical properties and radiative forcing of urban aerosols in Nanjing, China, Atmos. Environ., 83, 43–52, 2014a.

Figure Caption

Fig 1. Time series of the concentrations of PM_{10}, $PM_{2.5}$, and BC from September 2016 to February 2017 at Gulou site, Nanjing, China.

Fig 2. Seasonal variations of (a) BC, (b) $PM_{2.5}$, and (c) PM_{10}. Red markers represent the monthly averages at Gulou site, Nanjing, China.

Fig 3. 6-month mean diurnal variations of BC, $PM_{2.5}$, and PM_{10} at Gulou site, Nanjing, China from September 2016 to February 2017.

Fig.4 Time series of particles from September 2016 to February 2017 at Gulou site.

Fig 5. Seasonal variations of (a) O_3, (b) NO_x, (c) CO, and (d) NO_y. The 10, 25, 50, 75, and 90% percentile values of each are shown in black, and red markers represent the monthly averages.

Fig 6. 6-month mean diurnal variations of (a) trace gases and (b) UV (ultra-violate radiation) at Gulou site from September 2016 to February 2017.

Fig 7. Scatter plots of (a) O_3-NO_x color-coded with air temperature (T) and (b) $PM_{2.5}$-Vis color-coded with relative humidity (RH).

Fig 8. Scatter plots of (a) $PM_{2.5}$-O_3 and (b) BC-O_3 color-coded with air temperature (T).

Fig 9. Scatter plots of (a) O_3-UV and (b) $PM_{2.5}$-UV color coded with O_3.Fig 10. Scatter plots of (a) CO-NO_x, (b) $PM_{2.5}$-NO_x, and (c) BC-NO_x color-coded with O_3.

Fig 11. Clusters of 96 h back trajectories arriving at the study site at 100 m in 2016 fall.

Fig 12. The 10, 25, 50, 75, and 90% percentile values in each cluster of back trajectories in 2016

fall of (a) BC, (b) $PM_{2.5}$, (c) $PM_{2.5}/PM_{10}$, (d) CO, (e) O_3, (f) NO_y, (g) α_{ts}, and (h) ω_0. Black markers represent the averages.

Fig 13. Clusters of 96 h back trajectories arriving at the study site at 100m in 2016 winter.

Fig 14. The 10, 25, 50, 75, and 90% percentile values in each cluster of back trajectories in 2016 winter of (a) BC, (b) $PM_{2.5}$, (c) $PM_{2.5}/PM_{10}$, (d) CO, (e) O_3, (f) NO_y, (g) α_{ts}, and (h) ω_0. Black markers represent the averages.

Fig 15. Time series during December 3-6, 2016, for (a) $PM_{2.5}$, BC and O_3 with associated meteological parameters, trace gases and (b) optical parameters. Red markers represent O_3 over daily maximum average during winter. Weather charts on (c) 4th and (d) 5th December. (f) 96h backward trajectories analysis ending at 1200 UTC on 5th December

1478 **Table**

1479 Table 1 Measurements at Gulou site.

Measurement		Instrument	Resolution
Meteorological parameters	T (℃)	Thermo Instruments, THOM 1405-DF	
	P (atm)	Thermo Instruments, THOM 1405-DF	
	RH (%)	Thermo Instruments, THOM 1405-DF	
	Rainfall (mm)		
	Vis (m)	Visibility Meter, GSN-1	
	UV (W/m^2)		
Particles	BC (ng/m^3)	Aethalometer, Model AE-31	1 ng/m^3
	$PM_{2.5}$ ($\mu g/m^3$)	Thermo Instruments, THOM 1405-DF	0.1$\mu g/m^3$
	PM_{10} ($\mu g/m^3$)	Thermo Instruments, THOM 1405-DF	0.1$\mu g/m^3$
Gaseous pollutant	CO (ppb)	Thermo Instruments, TEI 48i	1 ppb
	NO_x (ppb)	Thermo Instruments, TEI 42i	0.4 ppb
	NO_y (ppb)	Thermo Instruments, TEI 42iY	0.4 ppb
	O_3 (ppb)	Thermo Instruments, TEI 49i	0.01 ppb
Optical parameters	SC (Mm^{-1})	Nephelometer, Aurora 3000	10^{-3} Mm^{-1}
	BSP (Mm^{-1})	Nephelometer, Aurora 3000	10^{-3} Mm^{-1}
	AAC (Mm^{-1})	Aethalometer, Model AE-31	10^{-3} Mm^{-1}

1480
1481

1482 Table 2 Statistics of general meteorological parameters at Gulou site for the 6-month period

1483 September 2016~ February 2017.

Month	Temp (℃)	Pres (hPa)	RH (%)	Rainfall (mm)	Vis (km)	UV (W/m^2)
Sep	24.88	996.97	69.41	2.34	11.84	10.36
Oct	18.37	1003.01	85.01	3.12	9.07	5.28
Nov	12.36	1007.87	77.15	1.19	8.99	5.67
Dec	8.74	1010.53	70.33	0.81	7.61	5.03
Jan	6.49	1010.89	70.65	0.59	9.23	4.94
Feb	7.72	1009.65	59.99	0.45	10.24	7.04

1484
1485
1486

Table 3 Statistics of the three particles during the study period at Gulou site, Nanjing, China

	SON	DJF	Cold seasons		
	Mean ± STD	Mean ± STD	Mean ± STD	Maximum	Minimum
BC (μg/m³)	2.126 ± 1.457	3.083 ± 1.827	2.602 ± 1.720	15.609	0.064
$PM_{2.5}$ (μg/m³)	43.1 ± 25.4	73.2 ± 40.0	58.2 ± 36.8	256.2	0.8
PM_{10} (μg/m³)	67.6 ± 39.1	105.0 ± 54.0	86.3 ± 50.8	343.4	1.1

Table 4 Statistics of trace gases during the study period

	SON	DJF	Cold seasons		
	Mean ± STD	Mean ± STD	Mean ± STD	Maximum	Minimum
CO (ppb)	753 ± 353	950 ± 388	851 ± 384	2852	176
NO_x (ppb)	21.4 ± 13.4	25.6 ± 15.5	23.5 ± 14.7	80.0	2.7
NO_y (ppb)	28.6 ± 20.5	37.0 ± 23.1	32.8 ± 22.3	158.4	3.6
O_3 (ppb)	42.3 ± 40.1	33.1 ± 24.4	37.7 ± 35.5	235.7	0.2

Table 5 Statistics of maximum and number of exceedances of O_3 and $PM_{2.5}$ compared with the National Ambient Air Quality Standards in China.

Aerosol	Mean ± STD (μg/m³)	Max (μg/m³)	N.o.E.
$PM_{2.5}$	58.2 ± 36.8	256.2	48
PM_{10}	86.3 ± 50.8	343.4	14
O_3	80.8 ± 71.8	235.7	37

N.o.E. of $PM_{2.5}$ accounts for days with 24 h average over 75 μg/m³. N.o.E. of PM_{10} accounts for days with 24 h average over 150 μg/m³. N.o.E of O_3 accounts for days with maximum 8 h average exceed 160 μg/m³.

Table 6 Statistics of aerosols at Gulou site with and without rainfall for the 6-month period September 2016~ February 2017

	With Rainfall			Without Rainfall		
Aerosols	Mean ± STD	Maximum	Minimum	Mean ± STD	Maximum	Minimum
BC (μg/m³)	1.676 ± 1.261	8.256	0.064	2.723 ± 1.735	15.608	0.211
$PM_{2.5}$ (μg/m³)	31.2 ± 27.6	218.4	1.2	61.9 ± 36.3	256.2	0.8
PM_{10} (μg/m³)	54.3 ± 44.8	307.3	3.9	89.1 ± 47.3	319.6	4.5
CO (ppb)	659 ± 240	2194	176	876 ± 392	2852	228
NO_x (ppb)	20.4 ± 12.7	75.5	2.9	23.9 ± 14.9	80	2.7
NO_y (ppb)	25.2 ± 16.8	110.3	3.6	33.8 ± 22.8	158.4	5.2
O_3 (ppb)	22.3 ± 17.1	81.7	0.3	39.7 ± 34.6	235.7	0.2

Figures

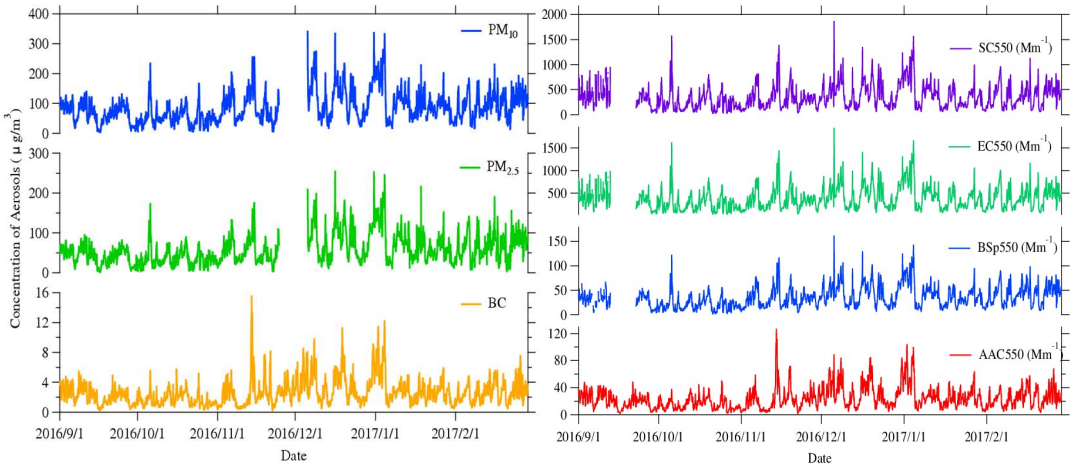

Fig 1. Time series of (a) concentrations and (b) optical properties of PM_{10}, $PM_{2.5}$, and BC from September 2016 to February 2017 at Gulou site, Nanjing, China.

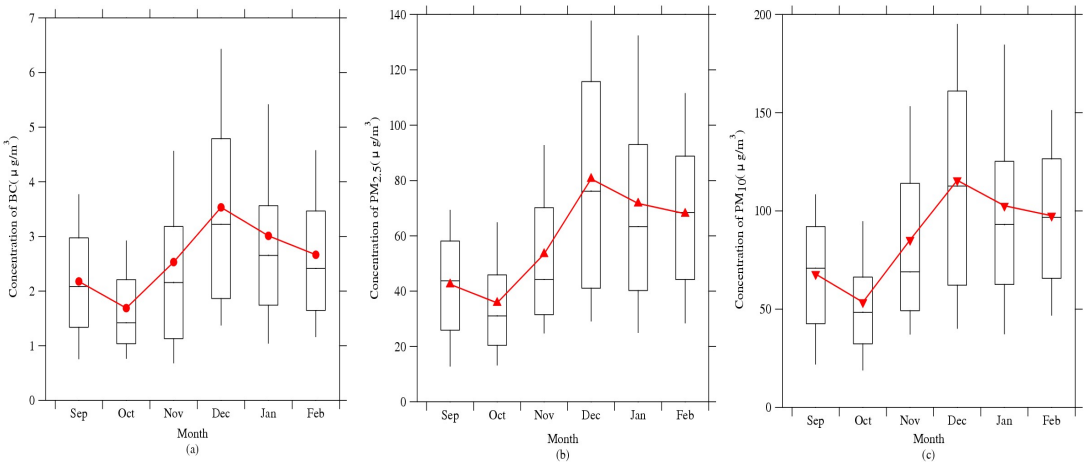

1518

1519 Fig 2. Seasonal variations of (a) BC, (b) $PM_{2.5}$, and (c) PM_{10}. Red markers represent the monthly

1520 averages at Gulou site, Nanjing, China.

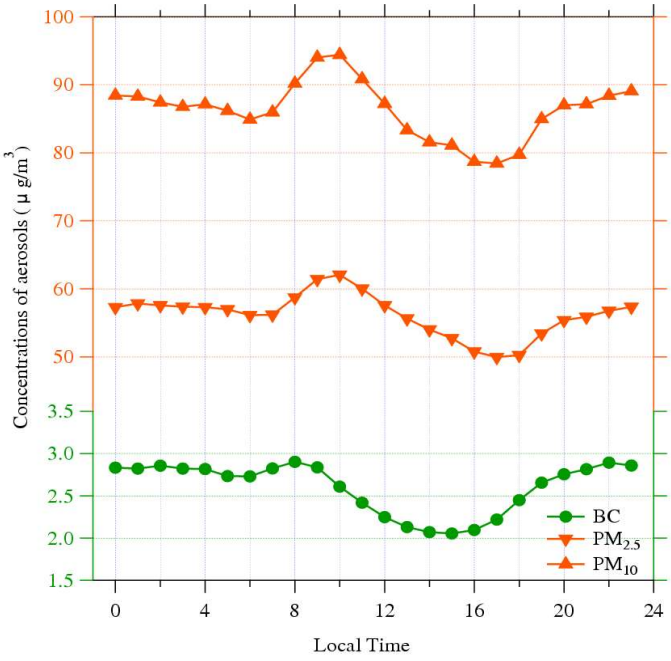

1521

1522 Fig 3. 6-month mean diurnal variations of BC, $PM_{2.5}$, and PM_{10} at Gulou site, Nanjing, China

1523 from September 2016 to February 2017

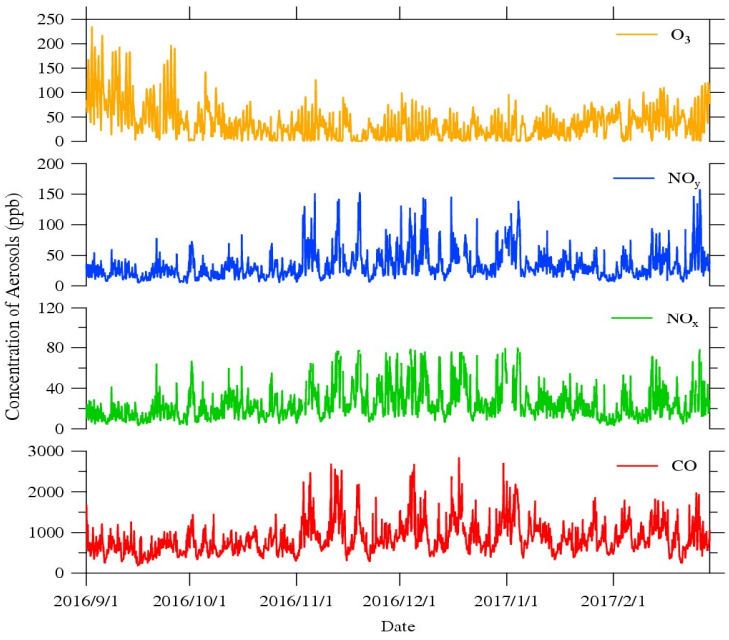

Fig.4 Time series of particles from September 2016 to February 2017 at Gulou site.

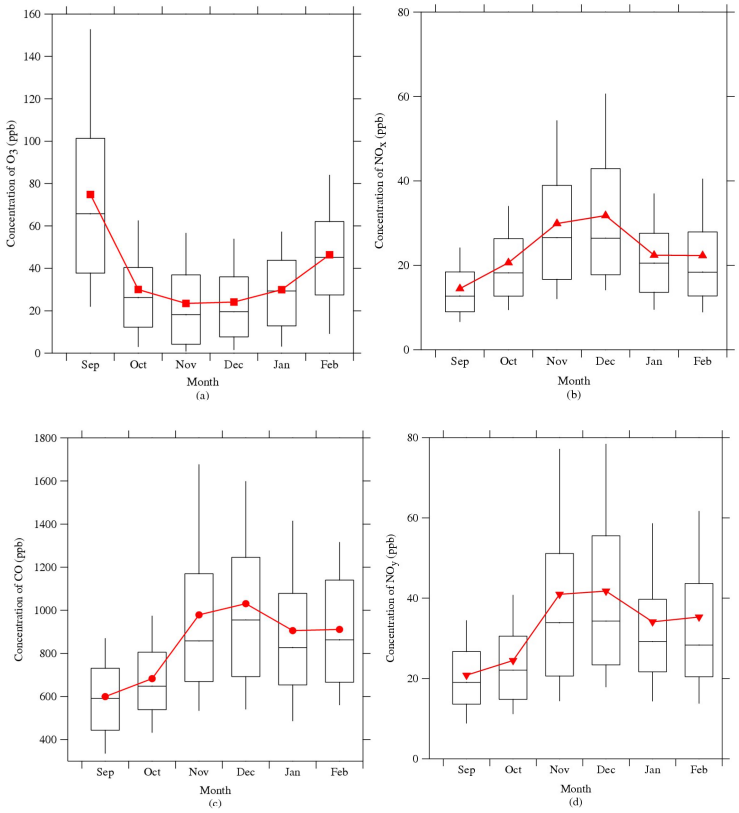

Fig 5. Seasonal variations of (a) O_3, (b) NO_x, (c) CO, and (d) NO_y. The 10, 25, 50, 75, and 90% percentile values of each are shown in black, and red markers represent the monthly averages.

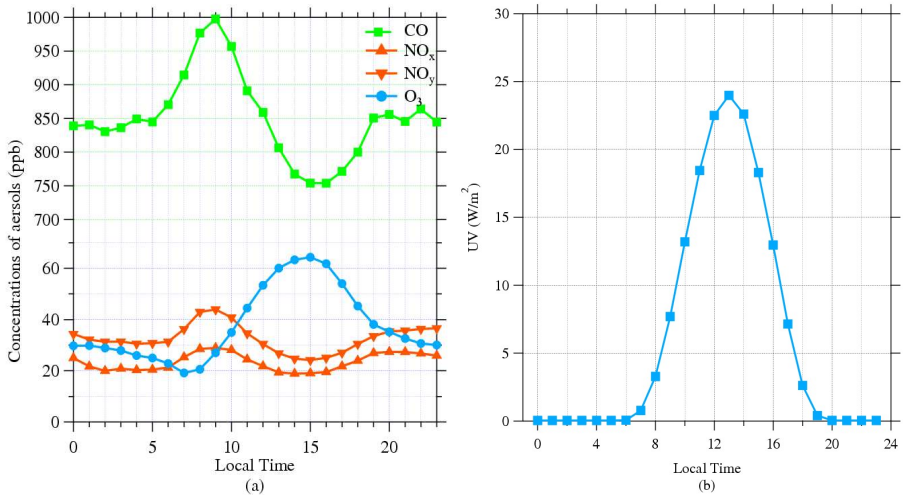

Fig 6. 6-month mean diurnal variations of (a) trace gases and (b) UV (ultra-violate radiation) at Gulou site from September 2016 to February 2017.

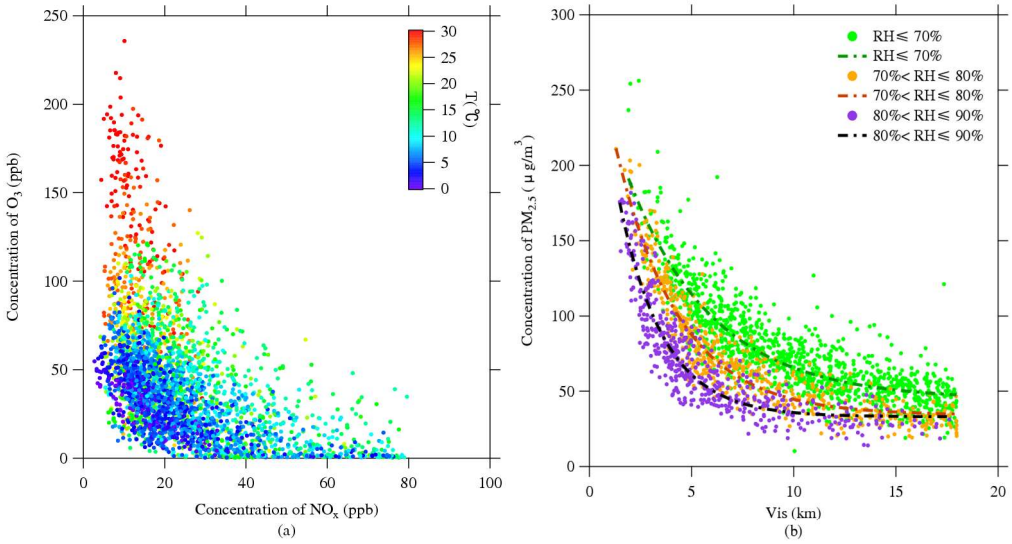

Fig 7. Scatter plots of (a) O_3-NO_x color-coded with air temperature (T) and (b) $PM_{2.5}$-Vis color-coded with relative humidity (RH).

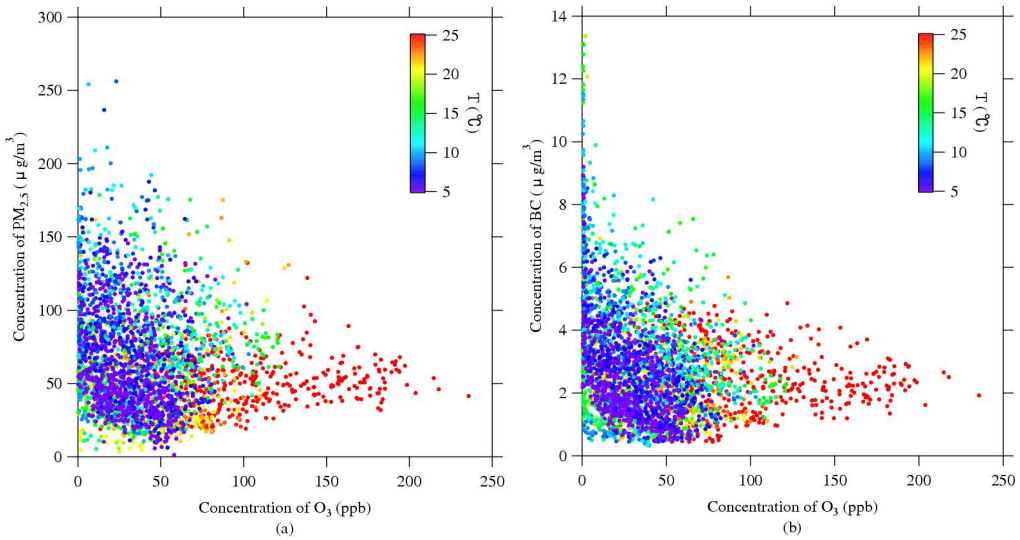

Fig 8. Scatter plots of (a) $PM_{2.5}$-O_3 and (b) BC-O_3 color-coded with air temperature (T).

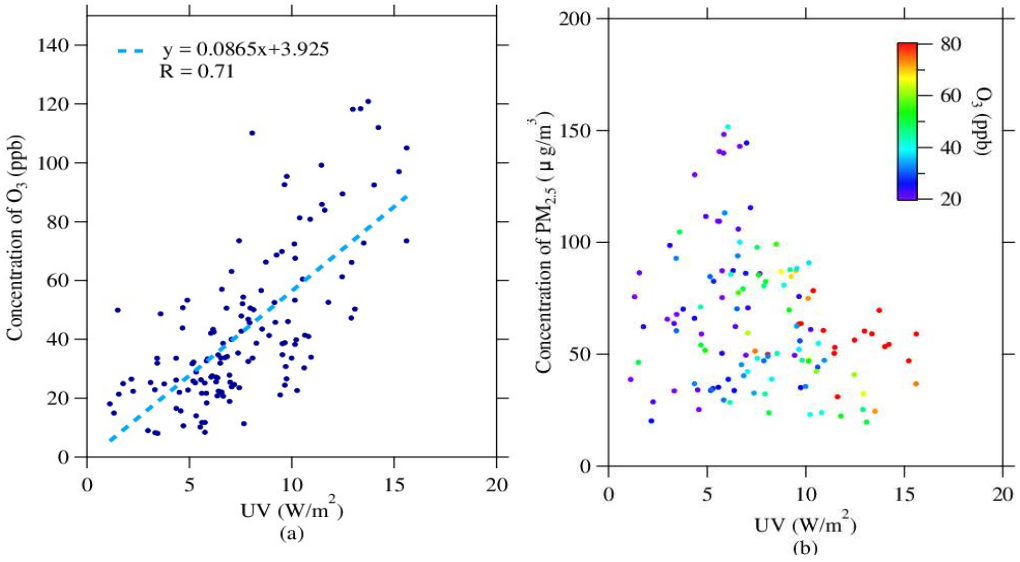

Fig 9. Scatter plots of (a) O_3-UV and (b) $PM_{2.5}$-UV color coded with O_3.

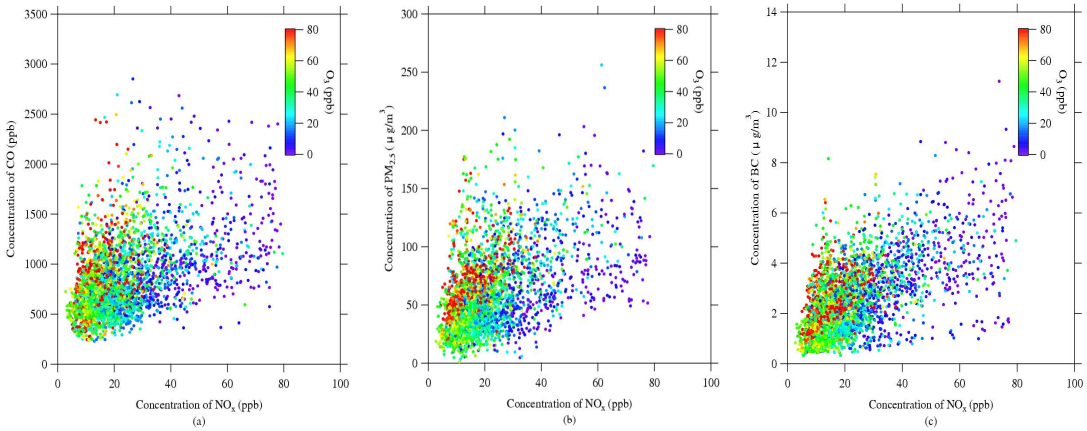

Fig 10. Scatter plots of (a) CO-NO_x, (b) $PM_{2.5}$-NO_x, and (c) BC-NO_x color-coded with O_3.

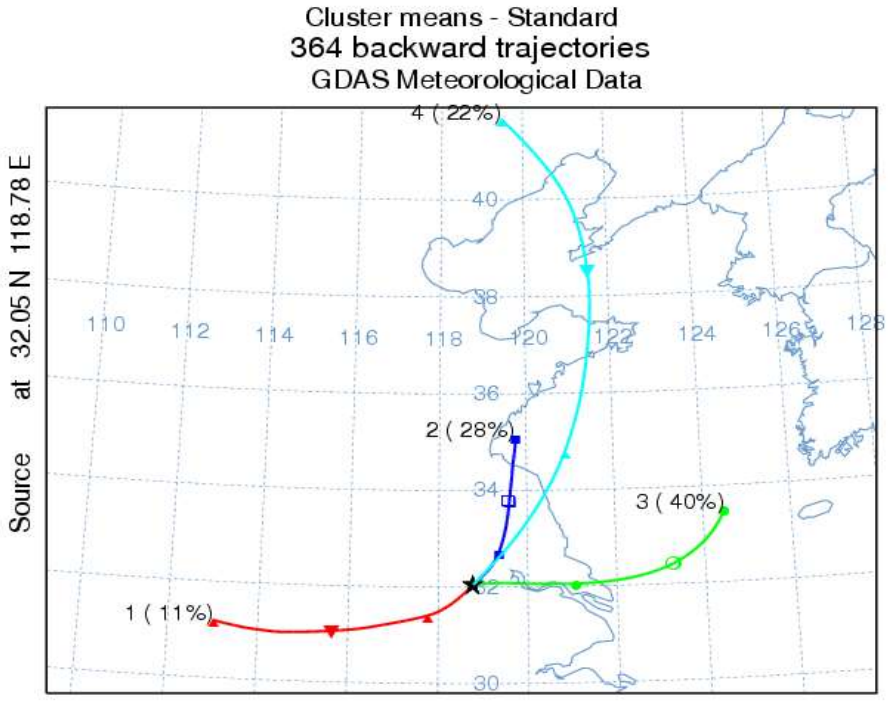

Fig 11. Clusters of 96 h back trajectories arriving at the study site at 100 m in 2016 fall.

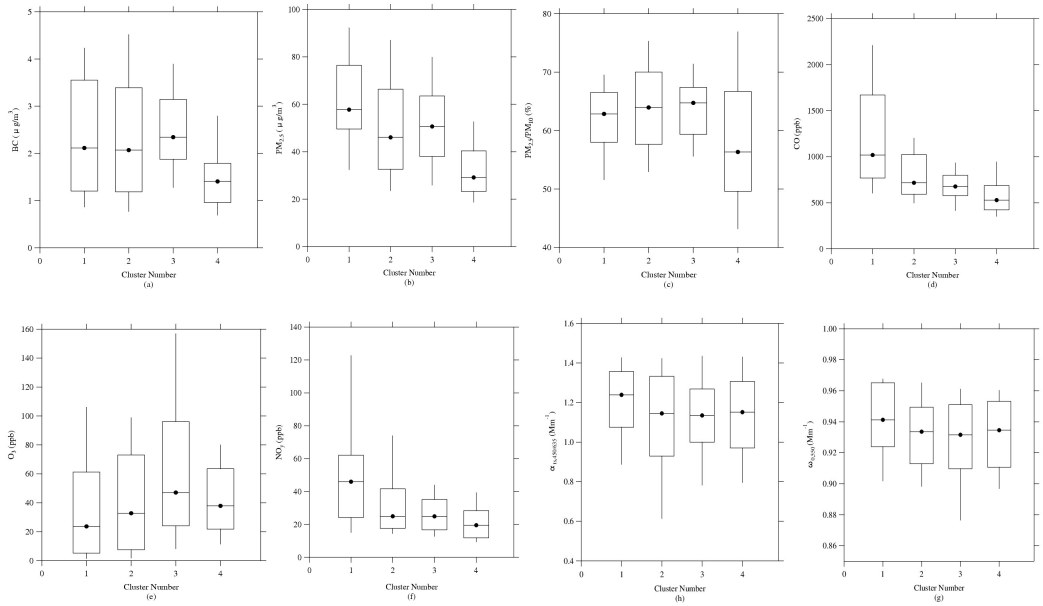

Fig 12. The 10, 25, 50, 75, and 90% percentile values in each cluster of back trajectories in 2016 fall of (a) BC, (b) $PM_{2.5}$, (c) $PM_{2.5}/PM_{10}$, (d) CO, (e) O3, (f) NO_y, (g) α_{ts}, and (h) ω_0. Black markers represent the averages.

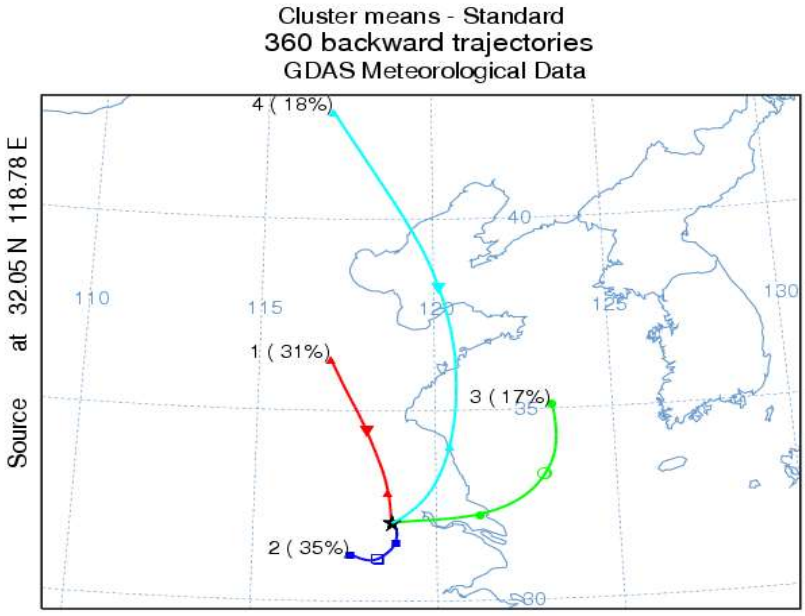

Fig 13. Clusters of 96 h back trajectories arriving at the study site at 100m in 2016 winter.

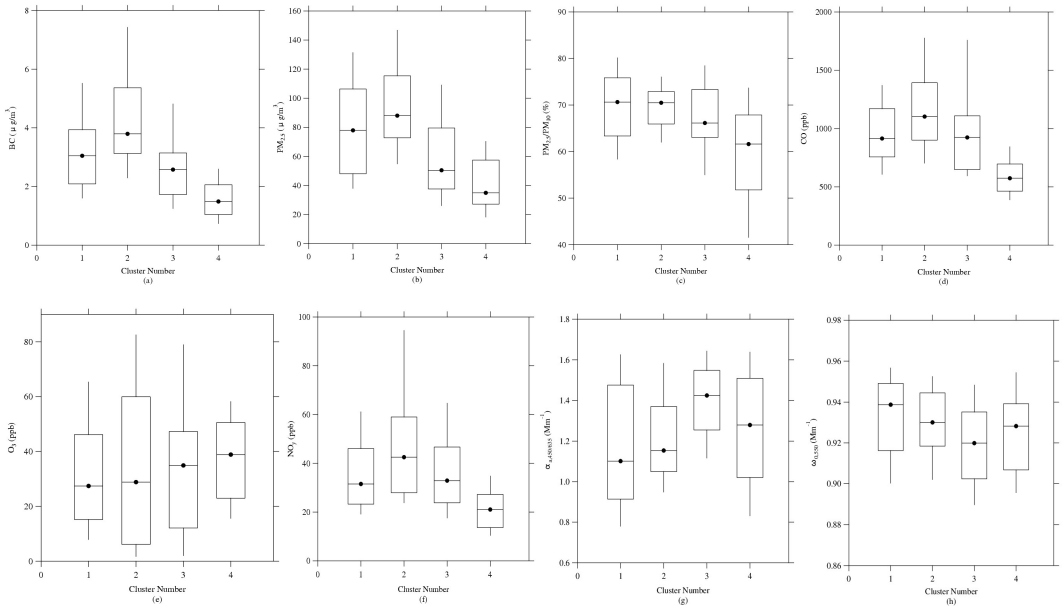

Fig 14. The 10, 25, 50, 75, and 90% percentile values in each cluster of back trajectories in 2016 winter of (a) BC, (b) $PM_{2.5}$, (c) $PM_{2.5}/PM_{10}$, (d) CO, (e) O_3, (f) NO_y, (g) α_{ts}, and (h) ω_0. Black markers represent the averages.

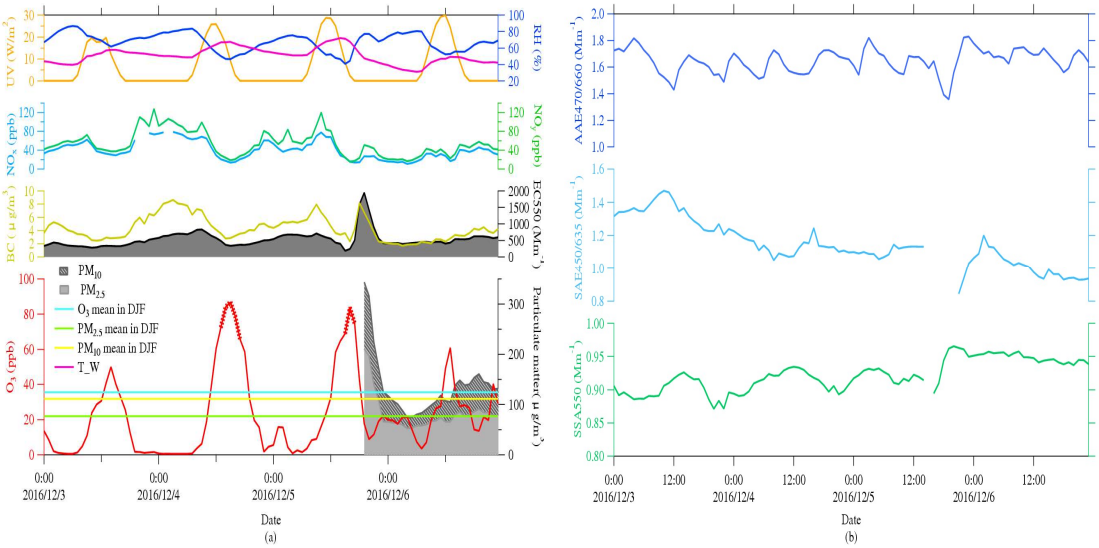

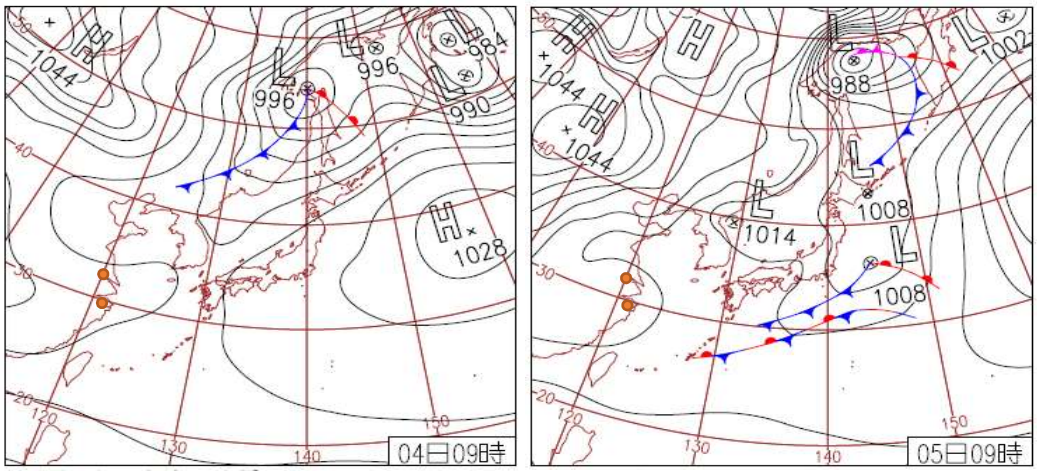

(c) (d)

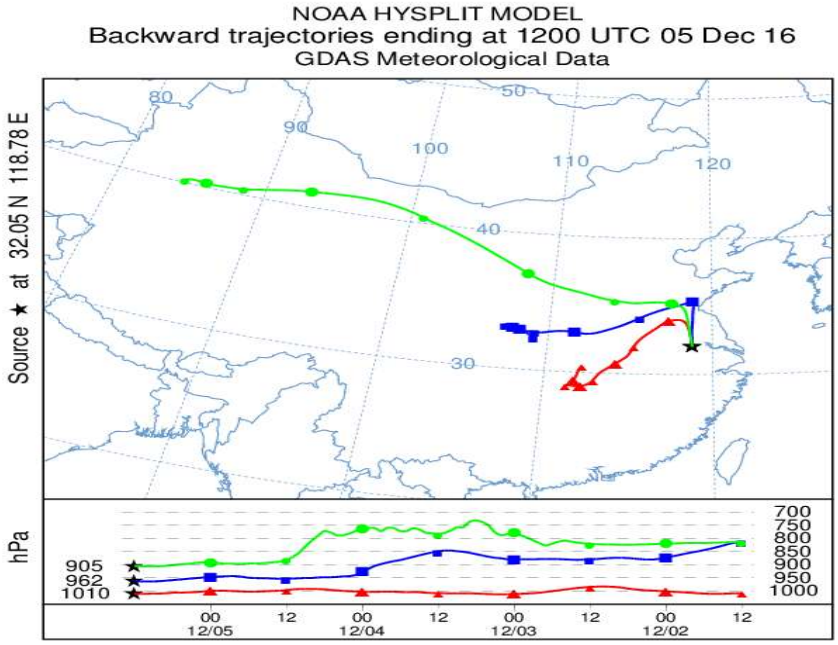

(f)

Fig 15. Time series during December 3-6, 2016, for (a) PM2.5, BC and O3 with associated meteological parameters, trace gases and (b) optical parameters. Red markers represent O3 over daily maximum average during winter. Weather charts on (c) 4th and (d) 5th December. (f) 96h backward trajectories analysis ending at 1200 UTC on 5th December.